Final Technical Report

USGS Award Number: G12AP20024

Extension of Database on Exceptional Strong Motion Accelerograms

John G. Anderson

Nevada Seismological Laboratory
and
Department of Geological Sciences and Engineering
University of Nevada
Reno, Nevada 89557
Phone: 774-784-1954
email: jga@unr.edu

January 1, 2012 - December 31, 2012

Abstract:

A collection of 445 of the strongest openly-available observed ground motion accelerograms has been compiled. The extended compilation includes 71 with PGA over 1 g and 41 with PGV over 1 m/s. The four strongest peak accelerations exceed 2 g, and the five strongest velocities exceed 1.5 m/s. Response spectra have been found for all records in this extended compilation. We geneate distribution functions of the amplitudes of exceptional ground motions, and for response spectra we find spectral amplitudes of about equal occurrence rate in addition to the current observational upper bounds. Perhaps it is just coincidental, but when the amplitude distributions are normalized by an estimate of the record time, they are similar to the hazard curves for a location of high seismic hazard (San Bernardino, California, based on the US National Hazard Map). Examples of exceptional records in different period ranges are shown, and the nature and cause of those motions is discussed. A strong source is an essential contribution in all cases. At long periods, exceptional ground motions are also generated by resonance in deep basins, sometimes very far from the sources. At intermediate and short periods, site resonance also frequently makes an important contribution. While non-linearity in soils generally tends to increase the site period, in rock and also at some soil sites, high frequency spikes on some of the records might also be generated by nonlinear processes near the stations.

Bibliography of publications supported in full or in part by this grant:

Anderson, J. G., (2012). "An Overview of the Largest Amplitudes in Recorded Ground Motions", Proceedings, 15th World Conference on Earthquake Engineering, 2012, 24-28 September 2012: Paper 3911.

Anderson, J. G., Nanjo, K. (2013). Distribution of Earthquake Cluster Sizes in the Western United States and in Japan, Bulletin of the Seismological Society of America, 103, No. 1, 412-423, doi:10.1785/0120100212.

Anderson, J. G., Kawase, H., Biasi, G. P., Brune, J. N. (2013). "Ground Motions in the Fukushima Hamadori, Japan, Normal Faulting Earthquake", Bull. Seism. Soc. Am., 103, 1935-1951.

John G. Anderson, Kazuki Koketsu, Hiroe Miyake (2013). Expanded Compilation and Statistics of Exceptional Ground Motions, submitted for publication.

Presentations supported by this grant:

"An Overview of the Largest Amplitudes in Recorded Ground Motions", J. G. Anderson, 15th World Conference on Earthquake Engineering, Lisbon, Portugal, September 2012.

" An Overview of the Largest Amplitudes in Recorded Ground Motions ", John G. Anderson, Kazuki Koketsu, Hiroe Miyaki, Annual Meeting, Seismological Society of America, Salt Lake City, Utah, April, 2013

" The Fukushima Hamadori, Japan, Earthquake: Extensive Ground Motion Data from a Surface-Rupturing Normal Fault ", John G. Anderson, Hiroshi Kawase, Glenn P. Biasi, James N. Brune, Shin Aoi, Annual Meeting, Seismological Society of America, Salt Lake City, Utah, April, 2013

Expanded Compilation and Statistics of Exceptional Ground Motions

John G. Anderson, Kazuki Koketsu, Hiroe Miyake

July 15, 2013

1 Abstract

A collection of 445 of the strongest openly-available observed ground motion accelerograms has been compiled. The extended compilation includes 71 with PGA over 1 g and 41 with PGV over 1 m/s. The four strongest peak accelerations exceed 2 g, and the five strongest velocities exceed 1.5 m/s. Response spectra have been found for all records in this extended compilation. We geneate distribution functions of the amplitudes of exceptional ground motions, and for response spectra we find spectral amplitudes of about equal occurrence rate in addition to the current observational upper bounds. Perhaps it is just coincidental, but when the amplitude distributions are normalized by an estimate of the record time, they are similar to the hazard curves for a location of high seismic hazard (San Bernardino, California, based on the US National Hazard Map). Examples of exceptional records in different period ranges are shown, and the nature and cause of those motions is discussed. A strong source is an essential contribution in all cases. At long periods, exceptional ground motions are also generated by resonance in deep basins, sometimes very far from the sources. At intermediate and short periods, site resonance also frequently makes an important contribution. While non-linearity in soils generally tends to increase the site period, in rock and also at some soil sites, high frequency spikes on some of the records might also be generated by nonlinear processes near the stations.

2 Introduction

Anderson (2008, 2010) compiled 255 strong motion records (from 82 earthquakes) for which either peak acceleration on one component exceeded 500 cm/s^2 or peak velocity on one component exceeded 50 cm/s. Anderson (2008, 2010) referred to such accelerograms as "exceptional", using the word exceptional with the same meaning as when one says it was "an exceptionally rainy month". That collection of records will be referred to as the "2010 compilation". The new compilation described in this paper is the "2013 compilation".

There are several motivations to compile the strongest records into one place. First, the results provide a context by which to evaluate the strong motion records from any earthquake. Second, the strongest records can be examined in order to understand those factors that contribute to the highest levels of shaking. Contributing factors that can be considered include tectonic and geological setting, focal mechanism, fault-station geometry including rupture kinematics, stress drop on the fault as a whole and on asperities, and site conditions (e.g. Strasser and Bommer, 2009). Third, if there are upper bounds to the peak acceleration or peak velocity caused by tectonic earthquakes, a compilation such as this will provide constraints on those bounds.

Another motivation for Anderson (2008, 2010) was to compare these results with the predictions of probabilistic seismic hazard analysis (PSHA) for the most critical facilities, such as large dams and nuclear power plants. PSHA results at very low probabilities (e.g. less than 10^{-4} per year) are quite sensitive to the aleatory uncertainty in ground motion prediction equations (e.g. Sabetta et al, 2005; Bommer and Abrahamson, 2006). Key examples come from seismic hazard analyses for nuclear facilities at Yucca Mountain, Nevada (Stepp, 2001) and in Switzerland (Abrahamson et al, 2002). At exceedance rates of 10^{-6}, 10^{-7}, and 10^{-8} per year, the Yucca Mountain study computed peak accelerations of 2.9 g, 5.8 g, and 11 g, and peak velocities of 3.0 m/s, 6.5 m/s, and 14 m/s (Stepp, 2001; Hanks et al, 2005, 2006; Wong et al, 2006). Evidence bearing on whether these results are reasonable may come from reexamination of how uncertainty is treated (e.g. Anderson and Brune, 1999) or from survival of precarious rocks (e.g. Brune, 1996, 1999). Knowledge of the largest motions that have been observed to date is also needed to inform an evaluation of these computations.

Anderson (2010) reported on the occurrence of peak acceleration and peak velocity, but not the values of others of the many parameters that are frequently used to measure the strength of ground motions. This paper extends the prior results to response spectra, and separately discusses horizontal and vertical components. This paper also adds 190 accelerograms, with the largest numbers of contributions from the 2011 Tohoku, Japan, earthquake and aftershocks.

This paper also considers the peak accelerations and peak velocities of the records after they have been filtered with a low-pass filter. There are several motivations for this step. Some of the earlier records are obtained on instruments with a more limited frequency response than newer instruments, so the application of, say, a 10 Hz low-pass filter to all records increases the meaningfulness of comparisons that include those records. In addition, some ground motion prediction equations model peak amplitudes from low-pass filtered accelerograms. For instance, Si and Midorikawa (1999, 2000), model records after applying a low-pass filter with a corner frequency of 10 Hz. Another motivation is for the evaluation of synthetic seismograms. For instance, several studies have now appeared that use finite element or finite difference modeling techniques to predict ground motions in southern California as a result of a rupture of the San Andreas fault (e.g. Olsen et al, 2006, 2008, 2009: Graves et al, 2008). These models have predicted peak velocities in band-limited records that exceed 100 cm/s, and acceleration response spectral amplitudes for a 3 s oscillator as high as 700 cm/s^2. It is interesting to be able to consider such records in the context of actual recordings of exceptional ground motions.

This paper describes the expanded compilation of exceptional ground motions, shows statistics for the highest values of the response spectra and for unfiltered and filtered seismograms, and then shows selected examples of records that are notable for their large amplitudes in various period bands.

3 Expanded Compilation

3.1 Methods

The criterion for adding records to this compilation include the following:

- The site is located at ground level, in a sufficiently small structure that the motions are dominated by incoming ground motions rather than structural response.
- The data and associated metadata are freely and easily available (generally over the internet but that is not essential).
- Peak acceleration exceeds 500 cm/s^2 or peak velocity exceeds 50 cm/s on any component.

To identify data, we have searched several potential sources of data, predominantly the Japan K-NET and KiK-net data at NIED and the Center for Engineering Strong Motion Data.

Earthquakes contributing records are listed in Tables 7 and 8 of the Appendix. Individual records are listed in subsequent Tables 9 to 17 in the Appendix. Every record located in these searches is included in this compilation, but there is no assurance that this compilation is complete. Nonetheless, with the 190 records added since the 2010 compilation, the sampling of phenomena causing exceptional ground motions is expanding in interesting ways so we suspect that fewer interesting and important phenomena have been left out.

When processed records were available from the agency, these were generally used. For records that have not been processed, such as from K-NET and KiK-net, records have been high-pass filtered with a corner frequency of 0.05 Hz or higher. Displacement response spectra ($SD\left(T_n\right)$) have been calculated for 280 oscillator periods (T_n) from 0.01 s to 100 s. The periods are incremented by 0.01 s from $T_n = 0.01$ s to $T_n = 0.99$ s, by 0.1s from $T_n = 1.0$ s to $T_n = 10.0$ s, and finally by 1.0s from $T_n = 11.0$ s to $T_n = 100.0$ s. For digital records with long durations, the time window was sometimes shortened. A Husid plot of the record was calculated as $e\left(\tau\right) = \int_0^{\tau} \left(a_1^2\left(t\right) + a_2^2\left(t\right) + a_3^2\left(t\right)\right) dt$, and the time window taken no shorter that the time during which this Husid plot increases from 0.1% to 98% of its final value.

The calculations to determine the displacement response (SD) with damping parameter $h = 5\%$ are carried out in the frequency domain. These spectral values are converted to pseudo-acceleration response (PSA) using the relation

$PSA = (2\pi/T_n)^2 SD(T_n)$ (e.g. Hudson, 1979). A cosine taper is applied to each seismogram component, the record is padded with zeros to the number of points corresponding to the next higher power of two, and then the record is again padded with zeros at the beginning and end to double its length and decrease wraparound effects in the Fourier transform. At each frequency, the oscillator response is computed for all three acceleration components. These three responses are used to find component response spectra, and then the horizontal components are rotated through a series of rotations to find rotD00, rotD50, and rotD100 (Boore, 2010), and GMrotD00, GMrotD50, and GMrotD100 (Boore et al, 2006). Note that rotD100 is the same as the peak horizontal vector response. These parameters are also found for peak acceleration and peak velocity.

This paper also addresses the effect of a low-pass filter on the seismograms. The original record may have signal present up to its Nyquist frequency, which is commonly 25 Hz, 50 Hz, or 100 Hz. The first passband considered is no filter, and although not always true this is treated as 25 Hz for the sake of plotting. A series of six low-pass filters were applied to each accelerogram in the 2013 collection. The applied filters are 2-pole Butterworth filters applied in the forward and reverse direction resulting in a zero net phase shift. The corner frequencies of the applied filters are 0.333, 0.5, 1, 2, 5, 10, and "25" (no filter) Hz.

Because instrumental noise on many of the records require filtering as part of the baseline correction, a high-pass filter was applied uniformly to all originally unprocessed records. Nevertheless, Figure 6 has extended the response spectra to very long periods. Since the long period of the response spectrum is asymptotic to the peak ground displacement the reliability of this extension depends on the quality of the integration to peak displacements. For small earthquakes recorded on modern instruments, this is probably not too bad, but with some older instruments the uncertainties are greater. The uncertainty will generally be no worse than uncertainty for the peak displacement. For large earthquakes for which some records have recorded static offsets, such as the Chi-Chi or Tohoku earthquakes, the long periods of the spectrum will be underestimated. Thus the results for periods longer than 3 seconds should probably be considered lower bounds for the current empirical upper bound (CEB) on response spectral amplitudes that will be discussed subsequently.

Some discussion of notation is needed. This paper uses the symbols A, V, or PSA to represent, generically, peak values of acceleration, velocity, or pseudo-acceleration response spectra. Subscripts designate the measurement details:

- $3C$ for 3-component vectors.
- H for horizontal vectors, equivalent to rotD100 of Boore (2010).
- LH for the larger horizontal component as recorded.
- GM for the geometric mean of horizontal components as recorded.

- $GMrotDxx$ where xx can represent 0%, 50%, or 100% as defined by Boore et al. (2006).

- $rotDxx$ where xx can represent 0%, 50%, or 100% as defined by Boore (2010).

While Anderson (2010) emphasized A_{3C} and V_{3C}, this paper emphasizes A_H, V_H, and PSA_H.

The 2013 compilation includes 72 records with $A_{3C} \geq 1g$, and 42 records with $V_{3C} \geq 1m/s$. This paper uses the moment magnitude, M_w when the seismic moment, M_0, is available, and for maximum consistency, the moment obtained from the Global Centroid-Moment-Tensor Project (Ekstrom et al, 2012) is preferred.

3.2 Earthquakes

At the time of this writing, the 2010 compilation has been expanded to 445 accelerograms (114 earthquakes). The most recent of the additional events occurred mostly in Japan in March and April, 2011. Figure 1 shows the locations of all earthquakes in the 2013 compilation, and the events are listed in Tables 7 and 8. The map shows that the distribution of sources is global, but also that data from Japan and California are the most prevalent. Figure 2 shows locations of Japanese earthquakes, Figure 3 shows locations of California and Nevada earthquakes, and Figure 4 shows locations of earthquakes from the Middle East and southern Europe that are included in this study.

This paper uses the moment magnitude, M_w whenever possible. The sourse for the M_w value is given in Tables 7 and 8. As this final report was nearing completion, the NGA West2 flatfile was released (Ancheta et al, 2013). Since Anderson (2010) used the value of M_w from the original NGA compilation as the first priority, this study updated M_w to values given in that study for most earthquakes. The next priorities were, in sequence, M_w obtained from the Global Centroid-Moment-Tensor Project (Ekstrom et al, 2012) website, M_w from the NIED F-net web site, M_w from PDE, or as a last resort M_{JMA} or m_b. Links to all of these web sites are given in the "Resources" section of this paper.

Figure 5 shows some statistical characteristics of this 2013 compilation. Figure 5A, giving magnitude of earthquakes in the compilation as a function of time, shows that the rate of data collection has increased with improved instrumentation. However, records from clusters of earthquakes resulting in enormous additions of new data, such as the 2011 Tohoku, Japan earthquake and associated aftershocks, are not expected to be obtained frequently with the current instrumentation levels. Below M˜6.5, where the most data is available to establish a trend, the empirical upper bound on peak accelerations in Figure 5B is showing only a weak magnitude dependence, as expected from, e.g., Hanks and McGuire (1981) and Baltay et al. (2013). The distribution of peak velocity below M˜6.5 in Figure 5C appears to be bounded by an increasing upper bound.

4 Statistics

4.1 Parameters from Unfiltered Records

Figure 6 shows the PSA response spectra (5% damping) of all 445 accelerograms used in this study. The current empirical upper bound (CEB) is highlighted in red. The CEB is caused by a contribution from many earthquakes. A total of 18 different seismograms contribute a segment of the CEB. The amplitudes at selected periods are given in Table 1.

Figure 6 also shows two lines (in yellow and green, respectively) identified as "PSA_{15}" and "PSA_{150}". The motivation for these lines is to show uniformly exceeded response spectral amplitudes. Thus for example, PSA_{15} could be defined as the spectral amplitudes that are equaled or exceeded 15 times. Anderson (2010) suggested that the 2010 compilation represented about 150,000 instrument-years of strong motion data collection. Thus in the 2010 compilation, PSA_{15} (2010) would approximate a ground motion amplitude exceeded at a rate of 10^{-4} per instrument-year (15 exceedances/150,000 years). Similarly, PSA_{150} in the 2010 compilation would approximate a ground motion amplitude exceeded at a rate of 10^{-3} per instrument-year. The yellow and green lines in Figure 6 show rounded and slightly smoothed values of these levels obtained from the 2010 compilation. Table 1 lists these values as "PSA[10^{-3} per instrument-year]" and "PSA[10^{-4} per instrument-year]". These curves make it possible to extend the definition of "exceptional ground motions" to the response spectral domain. New records were admitted into the 2013 compilation if PSA exceeded PSA[10^{-3} per instrument-year] of Table 1 at any period, but systematic searches on these parameters are more difficult so some records are undoubtedly overlooked. The threshold of "exceptional ground motions" of the "PSA[10^{-3} per instrument-year]" is shifted slightly from the threshold suggested by Anderson (2010), but the rate of $\sim 10^{-3}$ per instrument-year is perhaps slightly more intuitive, if not more meaningful.

Figures 7 and 8 show the distributions of PSA_H in the 2013 compilation, at 16 selected periods. Figure 9 shows the distribution for $\mathrm{PGA_H}$ and $\mathrm{PGV_H}$. The distributions are created by, for example, compiling the value of $\mathrm{PSA_H}$ at the selected period from all accelerograms in the database. The values are sorted from strongest to smallest. The strongest is assigned the rank of 1, the second is assigned the rank of 2, and so on. Thus the rank gives the number of records in the 2013 compilation with $\mathrm{PSA_H}$ equaling or exceeding the value corresponding to that record. Table 2 gives the values of PSA(T) for records with ranks 1-5. The table also gives the record number, which can be identified by consulting Tables 9-16 in the Appendix. Tables 3, 4, 5, and 6 give similar results for horizontal and vertical accelerations and velocities, including the effects of filtering on those records.

There is, of course, no physical reason to expect that these curves should follow any particular well-behaved mathematical shape. Figures 7 and 8 are plotted with a logarithmic y-axis primarily because this makes the most readable graph. This arbitrary choice of axes does suggest a test for a particular distribution, however. A linear relationship on these axes indicates that the number of accelerograms exceeding the value of $\mathrm{PSA_H}$ on the abscissa is decreasing exponentially with increasing amplitude. In fact, the figures suggest that the linear relationship works reasonably well for periods $T_n \leq 5.0s$. For $T_n \geq 10s$, the distributions are better described as concave upwards. The net effect is that there are more points at these periods with large amplitudes than might be expected from an exponential fit to the curves at smaller amplitudes. Figure 9 adds plots with log-log axes to test an alternative power law model for the distribution. For $\mathrm{A_H}$, the distribution is inconclusive: perhaps at the lowest ranks it is more linear on the log-log axes, suggesting that a power law model would be a better model in this range. But for higher ranks the exponential model looks better. For $\mathrm{V_H}$, the distribution is not particularly linear for either plotting style, suggesting that perhaps more than one process contributes to this distribution.

If one were to try to predict the numbers of exceedances in Figures 7, 8 and 9, the procedure would probably involve a weighted average of the exceedance rate curve obtained from a probabilistic seismic hazard analysis for each of the sites contributing a strong motion record. Considering that most of these records are obtained from active tectonic regions, Figure 9A shows as an experiment the exceedance rate curve for San Bernardino, California (Petersen et al., 2008) , which is near the San Andreas and San Jacinto faults in southern California. Since the 2010 compilation is estimated to represent 150,000 instrument-years, the San Bernardino curve is multiplied by 150,000, to give an estimate of the numbers of records expected to be obtained as a function of the peak acceleration. It is interesting that the San Bernardino hazard curve is parallel to the curve for numbers of exceedances of A_H. Perhaps this has little significance, but it could on the other hand be a weak indication that perhaps the shape of this hazard curve at a rate of as low as ~10^{-5} yr^{-1} is reasonable.

4.2 Parameters from Filtered Records

Figure 10 shows ranking of peak acceleration and peak velocity for both the horizontal vector and vertical components of filtered records. The five largest records of each type, together with a cross-reference to the identity of each accelerogram, are given in Tables 3 for A_H, Table 4 for V_H, Table 5 for A_V, and Table 6 for V_V. The PGA curves in Figure 10 are much more sensitive to the filter frequency than the PGV curves. This is expected since PGA is controlled more by the high frequency content in the accelerogram, so removal of the high frequencies generally causes the peak to decrease. The curves for peak velocity, on the other hand, are more closely clustered for filter frequencies of 2 Hz or greater, and only start to separate for the 0.5 Hz and 1 Hz filters. It is also notable that the PGV curves are very steep, with less than a factor of two in PGV separating the records at 2, 5, and 10 Hz filters with rank 2 from records of rank 60.

Ranking of the PSA_H from filtered records was introduced in Figures 7 and 8. One interesting feature of Figures 7 and 8 is how they differ as the corner frequency of the filter is reduced. Oscillators with periods substantially larger (e.g. a factor of two) than the filter period (the inverse of the filter frequency given in the figure) are insensitive to the filter frequncy, as seen by the convergence of the lines for oscillators with $T_S > 10s$. On the other hand, the distribution of peaks for the short period oscillators are bunched at small spectral response amplitudes, indicating that the high frequency spectral content on all of the records is limited.

5 Notable Examples

The 2013 compilation described here includes many records that show interesting and unusual phenomena. This section selects a few records of particular interest.

5.1 Largest Peak Accelerations and Velocities

Table 3 lists the largest unfiltered and filtered horizontal accelerations. Figure 11 shows a 5 second long segment of each of these accelerograms, rotated and shifted in time so that the peaks are aligned at the center of the plot. The peak on all five of these records is assymetrical, with a very short rise time, decreasing almost as rapidly initially after the peak, and then showing a "shoulder" before the decrease continues. This characteristic shape is conspicuously well developed on records 2, 3, and 4, but also present to a lesser extent on records 1 and 5.

The three components of the record with the largest value of A_H, recorded at the K-NET station Tsukidate (MYG004) in the 2011 Tohoku earthquake (M_w 9.1) (Kunugi et al., 2012; Aoi et al., 2012) are shown in Figure 12. The peak horizontal acceleration occurs in the midst of 3-4 cycles of high amplitudes with a fundamental period of about 4.0 sec. The horizontal packet contains visible higher frequency energy with a Fourier spectral peak at 12 Hz. This gives the appearance that resonance in a shallow layer contributes strongly to this exceptional peak acceleration by amplifying a strong incoming wave. A burst of high amplitude energy on the vertical components occurs simultaneously with several approximately harmonic cycles at the higher frequency of about 8 Hz. This puzzling feature occurs in the midst of the high amplitude motions from the rupture of the second strong motion generating area in the 2011 Tohoku earthquake (e.g. Kurihashi and Irikura, 2011). The station is at least 50 km from the causative fault, so these different frequencies cannot be P- and S-waves originating on the subduction thrust. If the higher frequency vertical motion were P-wave energy and the lower frequency horizontal motion were S-wave energy originating on the subduction fault, the P-wave packet should arrive at least 5 seconds before the S-wave packet. An explanation with greater chance of working is conversion of S- to P- at a sharp, shallow interface, where the S- resonates at 4 Hz, while the P-wave resonates at 8 Hz. The velocity model obtained from the K-NET web site has 3 layers. The top layer has $\beta_1 = 100$ m/s, and $\alpha_1 = 200$ m/s. If the layer thickness is 6.25 m, the fundamental frequency of both P- and S-waves would match the observations. The K-NET web site, and Kawase (2011) gives a thickness of only 1 - 1.2 m for this layer, which is insufficient. Thus nonlinearity and the involvement of deeper layers are necessary to generate these spectral peaks. (Kawase, 2011). Furthermore, for efficient conversion of S-waves to P-waves in a flat-ayered structure, the incidence angle of the energy must be very shallow (D. VonSeggern, personal communication, 2013), while in this case energy from the source region would have a near-vertical incidence angle in layeres below the hypothetical resonant layer. Thus two- or three-dimensional effects must be involved, generating energy that is perhaps propagating as surface waves to the station from some strong, nearby heterogeneity.

Records with ranks of 2, 3, and 4 have a characteristic shaped spike that causes the exceptional peak. Another feature of the second strongest, recorded at station AKTH04 in the 2008 June 13 Southern Iwate earthquake (M_W 6.9) is that several of the peaks preceding the high peak are flattened at a common acceleration that is characteristic of the record (Figure 13). This is most conspicuous on the east component, on which 8 of the 10 the positive peaks before and large west-oriented acceleration all have peaks of about 0.6 g, as illustrated on Figure 13. There are five more rounded westward peak acceleations of about 1.0g preceding the 2.5g peak. In the context of nonliner behavior of the near-surface geology, these approximate limits may not be accidental. Rather the flattened eastward peaks may be flattened at an acceleration where a layer below the surface yields to large shear stress, thus limiting peak acceleration. The sharp westward acceleration then could arise by some sort of strain-hardening mechanism, such as when the moving surface block encounters a stiff obstacle that abruptly stops its motion.

Figure 14 shows the three components of the record from station MYG012, recorded in the Tohoku earthquake. As with the station from MYG004, the high peak accelerations occur during the accelerations from the second strong motion generating area. Kawase (2011) suggests that both of these high peaks originate from the same source. Whether or not that is the case, the nature of these high peaks are very different from those in Figure 12. In this case, there are two similarly-shaped high peaks consistent with a block of crustal material twice starting to slide to the west and being stopped suddenly.

Figure 15 shows the five largest vertical accelerograms in the 2013 compilation. Aoi et al. (2008) and Yamada et al. (2009) have previously discussed the record from IWTH25 in the Southern Iwate earthquake of 2008 June 13. This record shows much higher peaks in the upwards direction than in the downwards direction. Aoi et al. (2008) suggest this is caused by a "trampoline effect". Yamada et al. (2009) suggest that it is a slapdown phase. Figure 15 shows that all five of the largest events shows asymetry, although perhaps not quite on the same scale. The downwards accelerations are often not quite the same as the acceleration of gravity, so these suggest that elastic moduli that are greater under compression than under extension are operating in all cases, although it is not clear that they go to zero under extension as in the proposals of Aoi et al. (2008) or Yamada et al. (2009).

Figure 16 shows the five largest horizontal velocities in the 2013 compilation.

The two largest are from stations TCU068 and TCU052, both on the hanging wall of the Chi Chi earthquake very near to the surface rupture (e.g. Oglesby and Day, 2001). These filtered records shown in Figure 16 do not recover the static offsets at the stations (e.g. Wu et al., 2001). The large velocities that are nonetheless recovered from these stations are representative of the dynamic slip near the rupture tip (Oglesby and Day, 2001; Dalguer et al., 2001; Wu et al., 2001). The other exceptional records are much smaller and have a much shorter duration. The Takatori station that recorded the Hyogo-ken Nanbu (Kobe) earthquake (M_{w} 6.9) was about 600 m from the vertical projection of the fault (e.g. Nakamura, 1995; Nakamura et al., 1996; Fukushima et al, 2000). Unique among these highest horizontal velocity records, the Kobe earthquake had a strike-slip mechanism. Among others Pitarka et al. (2000) have modeled the source of this earthquake. They find that the Takatori station is dominated by a pulse controlled by slip on the fault. However, the station is located on alluvium and they suggest that it was also amplified by the basin geometry. The Rinaldi Receiving Station (RRS) was located above the hanging wall of the Northridge earthquake (M_{w} 6.7), approximately updip from the hypocenter (e.g. Somerville et al., 1996). Wald et al. (1996) show that in the region updip from the hypocenter, most of the velocity time series are relatively strong and dominated by source processes. If the details in the Wald et al. (1996) inversion can be trusted, the RRS record may be enhanced some because after the largest slip in the rupture initially propagated updip at an angle slightly to the west of RRS for the first four seconds, between 4-6 seconds into the event the rupture extended towards the updip part of the fault where RRS is located, so there was possibly some forward directivity enhancing the velocity pulse. Based on Pitarka and Irikura (1996), RRS is also in a region where basin effects enhance the ground motions. Thus, the RRS reccord appears to be dominated by source processes but enhanced by basin amplification. Finally, the record from the 2007 Chuetsu earthquake, studied by Tokimatsu et al (2010), was also was very near the source, but amplified by basin effects. Liquefaction occurred at the site, but as in the case of the Niigata record mentioned above, the long periods seen in the velocity record are caused by direct S-waves from the nearby source.

In summary, the largest horizontal velocities are all dominated by direct pulses originating from the source. The Chi-Chi records are probably entirely dominated by slip below the station, while the other three are amplified as a result of being located on sediments. The largest vertical velocities are similar to the largest horizontal velocities, with the two largest dominated by the Chi Chi records and the next three from much smaller events with shorter periods. In this case however, some of the smaller events are recorded on analog instruments, and the integrations to velocity are less certain. Thus they are not shown here.

5.2 Long Period Ground Motions in Basins

Koketsu and Miyake (2008) identified several examples of large amplitude ground motions at long periods recorded at large distances that have been added in the 2013 compilation. It is interesting to consider these records in slightly more detail. These records illustrate the importance of understanding and predicting long period ground motions, as emphasized by Koketsu and Miyake (2008).

The 1985 Michoacan, Mexico, earthquake (M_w 8.0) generated devastating motions in Mexico City, about 400 km from the source region (e.g. Anderson et al, 1986). This is a classic example of damage at large distances caused by long period ground motions. Figure 17 shows the acceleration recorded at station SCT, located near a collapsed building in Mexico City 400 km from the epicenter. The peak accelerations on the horizontal components are only 167 cm/s^2 and 104 cm/s^2. This record is probably the most representative available record of the motions that destroyed large numbers of tall buildings, killing several thousand people in Mexico City. Figure 18 highlights the horizontal response spectrum from the SCT station, superimposed on the full set of response spectra in the 2013 compilation (also shown in Figure 6). The SCT spectrum at a period of 2 s is exceeded by only two other records in the database. The large amplitudes at SCT have been explained by various combinations of wave propagation from the subduction zone to Mexico City, basin effects and site amplification (e.g. Singh et al., 1988; Campillo et al., 1989; Kawase and Aki, 1989). Singh et al. (1989) suggest that the motions in the Mexico City basin are 75 times greater than those at an equivalent distance from the source along coastal Mexico.

The two other records that deserve special attention are the record from the K-NET station HKD129, recorded during the 2003 Tokachi-oki, Japan, earthquake (M_w 8.3) and the record from the station in Kawaguchi-cho from the 1964 Niigata, Japan, earthquake (M_{JMA} 7.5).

The long-period ground motions from the 2003 Tokachi-oki earthquake (M_w 8.3) were described by Hatayama et al. (2004) and Koketsu et al. (2005). The high amplitudes were particularly notable on several stations in the Yofutsu sedimentary basin at distances of 225-250 km from the epicenter of the earthquake. Koketsu et al. (2005) show that Fourier amplitudes at periods from about 5-8 seconds are particularly high at the K-NET station HKD129, 225 km from the epicenter (Figure 19). Therefore Figure 20 compares response spectra from this station with the response spectra in Figure 6. The PGA and PGV at HKD129 were 93 cm/s^2 and 33 cm/s, respectively. This figure shows that at the longest periods, the response spectrum is in about the highest 10-15% of the current set of exceptional accelerograms.

Strong motion records at Kawagishi-cho from the June 16, 1964 Niigata earthquake (M_{JMA} 7.5) were discussed by Kawasumi (1968) and Kudo et al. (2000). Kudo et al. (2000) review the extensive literature on this accelerogram, and provide a new digitization of the record. On this record, shown in Figure 21, PGA and PGV were, respectively, 164 cm/s^2 and 73.7 cm/s. Figure 22 compares the response spectra of this record with the response spectra in Figure 6. At periods between 5 and 6 seconds, this accelerogram is one of the three strongest records in the 2013 compilation. The epicenter of the earthquake was about 40-50 km north of the accelerometer, and the nearest part of rupture was likely nearer, based on the aftershock map shown by Kudo et al. (2000). Thus this station is not as distant as the examples in Figures 17 to 20. Kudo et al.

(2000) attribute the sudden decrease in the amplitudes of high frequency motions immediately after the peak motions, about 9 seconds after the instrument triggered, to liquefaction. Kudo et al. (2000) demonstrate that the long period motions after the change in record character due to liquefaction is the result of strong low-frequency radiation from the source amplified by the sediments of the Niigata basin.

6 Discussion

The 2013 compilation of exceptional ground motions includes 445 strong response spectra shown in Figure 6. The large increase in the number of records in 2011 is due to the well-recorded Tohoku earthquake. Obviously, earthquake clusters of such large magnitude are very rare. Thus the numbers of exceptional records added in this update, with 190 records added in four years, is anomalous.

Large crustal earthquakes are still very poorly represented in the 2013 compilation. The large amplitude, long period velocity pulse in the Chi Chi earthquake is unique in this compilation, but should be expected on the hanging wall of other large-magnitude dip-slip earthquakes. The hanging wall effect in large magnitude normal-faulting events is entirely unsampled.

Figures 7-10 show the distributions of response spectra and peak acceleration and velocity, using both unfiltered and filtered records. The filtered records should be useful for comparison with synthetic seismograms generated using finite elements or finite difference techniques that are limited to low frequencies by lack of knowledge of crustal structure, uncertain source dynamics, and computational limits.

Some members of the seismological and earthquake engineering community will remember a time when accelerations over $1g$ were considered impossible or extraordinarily remarkable. Now, five records have A_{3D} >$2g$. Three records have A_H over $2g$ on the horizontal component and another has A_V over $2g$ on the vertical component. Five records have $\mathrm{V_H}$>150 cm/s. There are over 80 accelerograms now with peak values in excess of 1g, and when low-pass filtered with corner frequencies of 10 Hz and 5 Hz, 30 and 8 records, respectively, remain with peaks over 1g. There are 40 records with PGV in excess of 100 cm/s, with few of those peaks reduced significantly by filters with corner frequency of 5 Hz or higher.

7 Conclusions

The causes of many of these exceptional records are not yet investigated. Still, it is clear that strong effects of the near-surface geology are very important for a large fraction of the records. At long periods, basins are clearly capable of causing enormous increases in ground motion amplitudes. As discussed by Koketsu and Miyake (2008) those effects can be extremely destructive to long-period structures. At shorter periods, shallow site-resonance can cause motions from a strong source to be amplified to exceptional ground motion levels. In addition, near-surface non-linearity appears to have generated high-frequency spikes in some of the strong motion records with the largest amplitudes. On the other hand, strong source effects appear to dominate the largest peak velocities in the 2013 compilation.

However, it must be expected that the current empirical upper bound on the response spectrum will be exceeded in future earthquakes. It would seem to be just a matter of time until very large crustal earthquakes will be recorded at much shorter distances to the fault, and on site conditions that strongly amplify the ground motions. Some of that current upper bound is set by records from the Tohoku earthquake, for which the fault is no closer than ~50 km from the stations. It also is just a matter of time before a subduction thrust event of comparable magnitude ruptures on a trench that is closer to the shoreline, causing greater motions than any seen in the Tohoku earthquake.

8 Data Sources

Locations and moment magnitudes and reports from the NGA West2 project are given in the NGWest2 flatfiles, available from the PEER web site (http://peer.berkeley.edu/ngawest2/, last accessed June 18, 2013). Seismic moment determined by the Global Centroid-Moment-Tensor (GCMT) Project is available from the GCMT web site (http://www.globalcmt.org/, last accessed June 18, 2013). Moment determined by the National Research Institute for Earth Science and Disaster Prevention (NIED) of Japan using the F-net data is available from the F-net web site (http://www.fnet.bosai.go.jp/event/search.php?LANG=en, last accessed June 18, 2013). The F-net web site was also used as the source for Japan Meteorological Agency (JMA) locations and origin times. The Preliminary Determination of Epicenters (PDE) catalog used for many locations outside of Japan, for some values of M_w, and for m_b when M_w is not available, is available on a U. S. Geological Survey web site (http://earthquake.usgs.gov/earthquakes/eqarchives/epic/, last accessed June 18, 2013). Data developed for the U. S. National Seismic Hazard Map is available from another US Geological Survey web site (http://earthquake.usgs.gov/hazards/, last accessed June 18, 2013).

Strong motion records from the United States and from selected major global earthquakes is available from the Center for Engineering Strong Motion Data (CESMD) web site (http://www.strongmotioncenter.org/, last accessed June 18, 2013). Older records can be found through the Consortium of Organizations for Strong Motion Observation System (COSMOS) web site (http://www.cosmos-eq.org/VDC/index.html, last accessed June 18, 2013). Japanese data from the K-NET and KiK-net stations is available from the NIED web site (http://www.kik.bosai.go.jp/, last accessed June 18, 2013).

9 Acknowledgements

The efforts of countless dedicated technicians, scientists, and the support of countless scientists, engineers, funding agencies, and other leaders, is gratefully acknowledged. The NGA database compiled by PEER was a starting point and valuable resource for this compilation. The NIED in Japan deserves special recognition for the K-NET and KiK-net strong motion networks, which has provided probably about half of the data used in this study.

JA thanks the Earthquake Research Institute at the University of Tokyo for hosting his visit during a sabbatical leave from the University of Nevada, and thanks the University of Nevada for allowing him to take a sabbatical leave. This study received partial support from the US Geological Survey NEHRP External Grants Program, under Award Number G12AP20024.

10 References

Abrahamson, N. A., P. Birkhauser, M. Koller, D. Mayer-Rosa, P. Smit, C. Sprecher, S. Tinic, and R. Graf (2002). PEGASOS—a comprehensive probabilistic seismic hazard assessment for nuclear power plants in Switzerland, in Proceedings of the Twelfth European Conference on Earthquake Engineering, London, paper no. 633.

Ancheta, T. D., R. B. Darragh, J. P. Stewart, E. Seyhan, W. J. Silva, B. S. J. Chiou, K. E. Wooddell, R. W. Graves, A. R. Kottke, D. M. Boore, T. Kishida, J. L. Donahue (2013). PEER NGA-West2 Database, Report PEER 2013/03, Pacific Earthquake Engineering Research Institute, University of California, Berkeley, California.

Anderson, J. G. (2008). Exceptional ground accelerations and velocities caused by earthquakes, Technical Report on Task ORD-FY06-022, http://www.osti.gov/bridge/product.biblio.jsp?osti_id=922664 (accessed December 2009), Nevada Seismological Laboratory, University of Nevada, Reno, Report Document Identifier TR-NQ- 022-2, Cooperative Agreement no. DE-FC28-04RW12232, Project Activity ORD-FY06-022, Final Technical Report Part B (for subtask 2), 126 pages.

Anderson, J. G. (2010). Source and site characteristics of earthquakes that have caused exceptional ground accelerations and velocities, Bulletin of the Seismological Society of America, Vol. 100, No. 1, pp. 1–36, February 2010, doi: 10.1785/0120080375.

Anderson, J. G., and J. N. Brune (1999). Probabilistic seismic hazard analysis without the Ergodic assumption, Seism. Res. Lett. 70, 19–28.

Anderson, J. G., J. Prince, J. N. Brune, and R. S. Simons (1982). Strong motion accelerograms, in J. G. Anderson and R. S. Simons, eds., The Mexicali Valley Earthquake of 9 June 1980, Newsletter Earthquake Eng. Res. Inst., 16, No. 3, May 1982, 79-83.

Anderson, J. G., P. Bodin, J. Brune, J. Prince, S. Singh, R. Quaas, M. Onate, and E. Mena, (1986). Strong ground motion and source mechanism of the Mexico earthquake of Sept. 19, 1985, Science 233, 1043-1049.

Aoi, S., T. Kunugi, W. Suzuki, N. Morikawa, H. Nakamura, S. Senna, and H. Fujiwara (2012), Strong motion characteristics of the 2011 Tohoku-Oki earthquake, Zisin, 64, 169-182 (in Japanese with English abstract).

Assimaki, D., W. Li, J. H. Steidl and K. Tsuda (2008). Site amplification and attenuation via downhole array seismogram inversion: a comparative study of the 2003 Miyagi-Oki aftershock sequence, Bull. Seism. Soc. Am 98, 301-330.

Baltay, A. S., T. C. Hanks and G. C. Beroza (2013). Stable stress-drop measurements and their variability: implications for ground-motion prediction, Bull. Seism. Soc. Am. 103, 211-222.

Bommer, J. J. and N. A. Abrahamson (2006). Review Article. Why Do Modern Probabilistic Seismic-Hazard Analyses Often Lead to Increased Hazard Estimates?, Bulletin of the Seismological Society of America, 96, 1967–1977.

Brune, J. N. (1996). Precariously balanced rocks and ground motion maps for southern California, Bull. Seism. Soc. Am. 86, 43–54.

Brune, J. N. (1999). Precarious rocks along the Mojave Section of the San Andreas Fault, California: constraints on ground motion from great earthquakes, Seism. Res. Lett. 70, 29–33.

Campillo, M., J. C. Gariel, K. Aki, and F. J. Sánchez-Sesma (1989). Destructive strong ground motion in Mexico city: Source, path, and site effects during great 1985 Michoacán earthquake, Bulletin of the Seismological Society of America 79, 1718-1735.

Dalguer, L. A., K. Irikura, J. D. Riera, and H. C. Chiu (2001). The Importance of the Dynamic Source Effects on Strong Ground Motion during the 1999 Chi-Chi, Taiwan, Earthquake: Brief Interpretation of the Damage Distribution on Buildings, Bulletin of the Seismological Society of America, 91, p. 1112-1127, doi:10.1785/0120000705.

Ekstrom, G., M. Nettles and A. M. Dziewonski (2012). The global CMT project 2004–2010: Centroid-moment tensors for 13,017 earthquakes, Physics of the Earth and Planetary Interiors 200–201, 1–9.

Engdahl, E.R., and A. Villaseñor, Global Seismicity: 1900–1999 (2002). in W.H.K. Lee, H. Kanamori, P.C. Jennings, and C. Kisslinger (editors), International Handbook of Earthquake and Engineering Seismology, Part A, Chapter 41, pp. 665–690, Academic Press.

Engdahl, E.R., R. van der Hilst, and R. Buland (1998). Global teleseismic earthquake relocation with improved travel times and procedures for depth determination, Bull. Seism. Soc. Am. 88, 722–743.

Fukushima, Y., K. Irikura, T. Uetake, and H. Matsumoto (2000). Characteristics of Observed Peak Amplitude for Strong Ground Motion from the 1995 Hyogoken Nanbu (Kobe) Earthquake, Bulletin of the Seismological Society of America, June 2000, v. 90, p. 545-565, doi:10.1785/0119990066.

Fukuyama, E., S. Ishida, D. S. Dreger and H. Kawai (1998) Automated seismic moment tensor determination by using on-line broadband seismic waveforms, Zisin (J. Seismol. Soc. Jpn) Ser. 2, 51, 149-156 (in Japanese with English abstract).

Hatayama, K., S. Zama, H. Nishi, M. Yamada, Y. Hirokawa, and R. Inoue (2004). Long-period strong ground motion and damage to oil storage tanks due to the 2003 Tokachi-oki earthquake, Zisin, 57, 83-103 (in Japanese with English abstract).

Graves, R. W., B. T. Aagaard, K. W. Hudnut, L. M. Star, J. P. Stewart, and T. H. Jordan, Broadband simulations for M 7.8 southern San Andreas earthquakes: Ground motion sensitivity to rupture speed (2008). Geophys. Res. Lett., 35, 22, doi:10.1029/2008GL035750, 2008.

Hanks, T. C. and R. K. McGuire (1981). The character of high-frequency strong ground motion, Bull. Seism. Soc. Am. 71, 2071-2095.

Hanks, T. C., N. A. Abrahamson, M. Board, D. M. Boore, J. N. Brune and C. A. Cornell (2005). Observed ground motions, extreme ground motions, and physical limits to ground motions, in P. Gulkan and J. G. Anderson (eds.), Directions in Strong Motion Instrumentation, NATO Science Series IV. Earth and Environmental Sciences Vol. 58, Springer, Dordrecht, The Netherlands, 55-59.

Hanks, T. C., N. Abrahamson, M. Board, D. Boore, J. Brune, and A. Cornell (2006).Workshop on extreme ground motion at Yucca Mountain, U.S. Geol. Surv. Open-File Rept. OF2006-1277.

Hudson, D. E. (1979). Reading and interpreting strong motion accelerograms, Earthquake Engineering Research Institute, Berkeley, California, 112 pages.

Ide, S., M. Takeo, and Y. Yoshida (1996). Source process of the 1995 Kobe earthquake: Determination of spatio-temporal slip distribution by Bayesian modeling, Bulletin of the Seismological Society of America, June 1996, v. 86, p. 547-566.

Kamae, K. and K. Irikura (1998). Source model of the 1995 Hyogo-Ken Nanbu earthquake and simulation of near-source ground motion, Bulletin of the Seismological Society of America, April 1998, v. 88, p. 400-412.

Kawase, H. (2006). Site Effects Derived from Spectral Inversion Method for K-NET, KiK-net, and JMA Strong-Motion Network with Special Reference to Soil Nonlinearity in High PGA Records, Bull. Earthq. Res. Inst., Univ. Tokyo, Vol. 81, 309-315, 2006.12.

Kawase, H. (2011). Strong motion characteristics and their damage impact to structures during the off Pacific Coast of Tohoku earthquake of March 11, 2011; how extraordinary was this M9.0 earthquake, in Proceedings, 4th IASPEI/IAEE International Symposium: Effects of Surface Geology on Seismic Motion, August 23-26, 2011, University of California Santa Barbara.

Kawase, H. and K. Aki (1989). A study on the response of a soft basin for incident S, P, and Rayleigh waves with special reference to the long duration observed in Mexico City, Bulletin of the Seismological Society of America 79, 1361-1382.

Kawase, H., and H. Matsuo (2004). Amplification Characteristics of K-NET, KiK-NET, and JMA Shindokei Network Sites based on the Spectral Inversion Technique, 13th World Conference on Earthquake Engineering, Vancouver, Canada, Paper No.454, 2004.8.

Kawasumi, H. (1968). Introduction. In General Report on the Niigata Earthquake of 1964, H. Kawasumi, Editor-in-Chief, p.1-6, Tokyo Electrical Engineering College Press, Tokyo, Japan, 1968. http://www.iris.edu/seismo/quakes/1964niigata/

Koketsu, K. and H. Miyake (2008). A seismological evaluation of long-period ground motion, J. Seismology 12, 133-143, DOI 10.1007/s10950-007-9080-0.

Koketsu, K., K. Hatayama, T. Furumura, Y. Ikegami, and S. Akiyama (2005). Damaging long-period ground motions from the 2003 MW=8.3 Tokachi-oki, Japan, earthquake, Seismol. Res. Lett. 76, 67-73.

Kudo, K., T. Uetake and T. Kanno (2000). Re-evaluation of nonlinear site response during the 1964 Niigata earthquake using the strong motion records from at Kawagishi-cho, Niigata City, Proceedings, Proceedings, 12th World Conference on Earthquake Engineering, Paper 0969.

Kunugi, T., S. Aoi, W. Suzuki, H. Nakamura, N. Morikawa, and H. Fujiwara (2012). Strong motions of the 2011 Tohoku-Oki earthquake, Natural Disaster Research Report of NIED, 48, 63-72 (in Japanese with English abstract). http://dil-opac.bosai.go.jp/publication/nied_natural_disaster/index-e.html.

Kurihashi, S and K Irikura (2011) Source model for generating strong ground motions during the 2011 off the Pacific Coast of Tohoku earthquake, Earth Planets Space, Special Issue, 63, 571-576.

Nakamura, Y. (1995). Waveform and its analysis of the 1995 Hyogo-Ken-Nanbu earthquake, JR Earthquake Information No.23c, Railway Technical Research Institute (in Japanese).

Nakamura, Y., F. Uehan, and H. Inoue (1996). Waveform and its analysis of the 1995 Hyogo-Ken-Nanbu earthquake (II), JR Earthquake Information, No.23d, Railway Technical Research Institute (in Japanese).

Oglesby. D. D. and Steven M. Day (2001). Fault Geometry and the Dynamics of the 1999 Chi-Chi (Taiwan) Earthquake, Bulletin of the Seismological Society of America, October 2001, v. 91, p. 1099-1111, doi:10.1785/0120000714.

Olsen, K. B., S. M. Day, J. B. Minster, Y. Cui, A. Chourasia, M. Faerman, R. Moore, P. Maechling, and T. Jordan (2006). Strong shaking in Los Angeles expected from southern San Andreas earthquake, Geophys. Res. Lett., 33, 7, doi:10.1029/2005GL025472, 2006.

Olsen, K. B., S. M. Day, J. B. Minster, Y. Cui, A. Chourasia,D. Okaya, P. Maechling, and T. Jordan (2008). TeraShake2: Spontaneous Rupture Simulations of Mw 7:7 Earthquakes on the Southern San Andreas Fault, Bulletin of the Seismological Society of America, Vol. 98, No. 3, pp. 1162–1185, June 2008, doi: 10.1785/0120070148.

Olsen, K. B., et al. (2009), ShakeOut-D: Ground motion estimates using an ensemble of large earthquakes on the southern San Andreas fault with spontaneous rupture propagation, Geophys. Res. Lett., 36, L04303, doi:10.1029/2008GL036832.

Petersen, Mark D., Frankel, Arthur D., Harmsen, Stephen C., Mueller, Charles S., Haller, Kathleen M., Wheeler, Russell L., Wesson, Robert L., Zeng, Yuehua, Boyd, Oliver S., Perkins, David M., Luco, Nicolas, Field, Edward H., Wills, Chris J., and Rukstales, Kenneth S., 2008, Documentation for the 2008 Update of the United States National Seismic Hazard Maps: U.S. Geological Survey Open-File Report 2008–1128, 61 p.

Pitarka, A. and K. Irikura (1996). Basin structure effects on long-period strong motions in the San Fernando Valley and the Los Angeles Basin from the 1994 Northridge earthquake and an aftershock, Bulletin of the Seismological Society of America, February 1996, v. 86, p. S126-S137.

Pitarka, A., K. Irikura, T. Iwata, and H. Sekiguchi (1998). Three-dimensional simulation of the near-fault ground motion for the 1995 Hyogo-Ken Nanbu (Kobe), Japan, earthquake, Bulletin of the Seismological Society of America, April 1998, v. 88, p. 428-440.

Sabetta, F., A. Lucantoni, H. Bungum and J. J. Bommer (2005). Sensitivity of PSHA results to ground motion prediction relations and logic-tree weights, Soil Dynamics and Earthquake Engineering 25, 317-329.

Singh, S. K., E. Mena, and R. Castro (1988). Some aspects of source characteristics of the 19 September 1985 Michoacan earthquake and ground motion amplification in and near Mexico City from strong motion data, Bulletin of the Seismological Society of America 78, 451-477.

Somerville, P., C. Saikia, D. Wald, and R. Graves (1996). Implications of the Northridge earthquake for strong ground motions from thrust faults, Bulletin of the Seismological Society of America, February 1996, v. 86, p. S115-S125.

Stepp, J.C., I. Wong, J. Whitney, R. Quittmeyer, N. Abrahamson, G. Toro, R. Youngs, K. Coppersmith, J. Savy, and T. Sullivan (2001). Probabilistic Seismic Hazard Analyses for Ground Motions and Fault Displacement at Yucca Mountain, Nevada, Earthquake Spectra, 17, 113-151.

Strasser, F. O. and J. J. Bommer (2009). Large-amplitude ground-motion recordings and their interpretations, Soil Dynamics and Earthquake Engineering 29, 1305-1329.

Tokimatsu, K., K. Katsumata, and H. Arai (2010). Simulation of strong ground motions at K-NET Kashiwazaki during the 2007 Niigata-ken Chuetsu-oki earthquake, Proceedings of the 7th International Conference on Urban Earthquake Engineering and the 5th International Conference on Earthquake Engineering, 457-461.

Wald, D. J., T. H. Heaton, and K. W. Hudnut (1996). The slip history of the 1994 Northridge, California, earthquake determined from strong-motion, teleseismic, GPS, and leveling data, Bulletin of the Seismological Society of America, February 1996, v. 86, p. S49-S70.

Wong, I., W. Silva, P. Thomas, R. Quittmeyer, M. Dober, C. Law Pattanapong, R. Lee, G. Toro, K. Stokoe, and J. C. Stepp (2006). Development of earthquake ground motions for Yucca Mountain, paper number 1420, Proceedings of the 8th U.S. National Conference on Earthquake Engineering, April 18–22, 2006, San Francisco, California.

Wu, C., M. Takeo, and S. Ide (2001). Source Process of the Chi-Chi Earthquake: A Joint Inversion of Strong Motion Data and Global Positioning System Data with a Multifault Model, Bulletin of the Seismological Society of America, October 2001, v. 91, p. 1128-1143, doi:10.1785/0120000713.

11 Author Affiliations

John G. Anderson*, Kazuki Koketsu and Hiroe Miyake,

University of Tokyo, Earthquake Research Institute, 1-1-1 Yayoi, Bunkyo-Ku, Tokyo 113-0032, Japan.

*on leave from Nevada Seismological Laboratory and Department of Geological Sciences and Engineering, University of Nevada, Reno, Nevada 89557, United States.

12 Tables

Table 1: Values of 5% damped PSA, in units of cm/s^2, with estimated exceedance rates per instrument year of ~10^{-3} and ~10^{-4}, respectively, and the current empirical upper bound of PSA.

T_n	$10^{-3}/inst-yr$	$10^{-4}/inst-yr$	Current Empirical Upper Bound
0.01	600	1200	2740.1
0.02	600	1400	2887.7
0.03	700	1500	3855.1
0.05	800	1900	6376.8
0.1	1100	2600	4129.1
0.2	1200	3000	7778.4
0.3	1100	2800	6484.4
0.5	700	2000	3604.3
1	400	1500	2601.7
2	150	650	1293.5
3	70	470	752.42
5	30	220	438.76
10	6	55	283.29
20	1.3	8.5	53.064
50	0.2	1.3	7.9261
100	0.055	0.35	1.9153

Table 2: Largest values of 5% damped $PSA(T_n)$ in the 2013 compilation, for selected oscillator periods (T_n). See Tables 9 to 17 to identify the accelerogram from the record number (Rec.) given here.

	Oscillator Period							
	$T_n = 0.01$ s		$T_n = 0.02$ s		$T_n = 0.03$ s		$T_n = 0.05$ s	
Rank	Peak, cm/s^2	Rec.	Peak, cm/s^2	Rec.	Peak, cm/s^2	Rec.	Peak, cm/s^2	Rec.
1	2809.2	350	2998.3	350	4211.4	350	5871.7	350
2	2029.9	356	2499.5	6	3023.3	226	5593.4	416
3	1980.3	80	2174.3	356	2635.4	416	3629	6
4	1873	333	2167.3	226	2550.8	6	3616.4	226
5	1846.9	357	2028.9	80	2451.9	47	3454	80
	Oscillator Period							
	$T_n = 0.1$ s		$T_n = 0.2$ s		$T_n = 0.3$ s		$T_n = 0.5$ s	
Rank	Peak, cm/s^2	Rec.	Peak, cm/s^2	Rec.	Peak, cm/s^2	Rec.	Peak, cm/s^2	Rec.
1	4387.9	186	7444.1	350	6434.7	333	4284.5	231
2	4340	83	6032.5	414	5966	350	3574.8	312
3	4292.3	326	5620.7	232	5412.5	338	3263	395
4	4248.8	80	5297.2	168	5311.6	192	3011	166
5	4071.7	93	4892.7	192	4936.7	395	2980.8	80
	Oscillator Period							
	$T_n = 1$ s		$T_n = 2$ s		$T_n = 3$ s		$T_n = 5$ s	
Rank	Peak, cm/s^2	Rec.	Peak, cm/s^2	Rec.	Peak, cm/s^2	Rec.	Peak, cm/s^2	Rec.
1	2740.5	108	1538.7	257	759	257	466.84	122
2	2592.6	131	1402.1	86	610.32	40	433.4	120
3	2249.9	252	1187.3	131	584.21	116	360.59	110
4	1952.5	72	1134.6	29	577.39	267	358.69	116
5	1856.4	65	1098.8	288	559.75	75	335.37	109
	Oscillator Period							
	$T_n = 10$ s		$T_n = 20$ s		$T_n = 50$ s		$T_n = 100$ s	
Rank	Peak, cm/s^2	Rec.	Peak, cm/s^2	Rec.	Peak, cm/s^2	Rec.	Peak, cm/s^2	Rec.
1	322.25	122	65.505	122	7.4501	122	2.3905	57
2	209.03	116	45.641	116	6.1875	57	1.4687	122
3	134.93	40	28.741	51	5.4665	116	1.3211	51
4	90.541	139	23.101	57	2.8964	39	1.1578	116
5	86.074	113	22.869	203	2.7351	203	1.0732	5

Table 3: Five largest values of peak horizontal accelerations in the 2013 compilation. Peaks are given for original records, listed under the 25 Hz. category, and for records after application of low-pass filters with various corner frequencies. See Tables 9 to 17 to identify the accelerogram from the record number (Rec.) given here.

	Low Pass Filter Corner Frequency					
	25 Hz		10 Hz		5 Hz	
Rank	Peak, cm/s^2	Rec.	Peak, cm/s^2	Rec.	Peak, cm/s^2	Rec.
1	2761.5	350	2292.2	350	1483.3	350
2	2504.4	262	1591.8	54	1172.8	312
3	1984.7	356	1587.6	262	1142.5	231
4	1965.2	80	1534.6	80	1134.3	80
5	1858.8	333	1461.1	333	1107.9	108

	Low Pass Filter Corner Frequency							
	2 Hz		1 Hz		0.5 Hz		1/3 Hz	
Rank	Peak, cm/s^2	Rec.	Peak, cm/s^2	Rec.	Peak, cm/s^2	Rec.	Peak, cm/s^2	Rec.
1	821.8	108	463.1	86	228.6	257	158.7	122
2	789.3	72	442.9	226	223.9	116	139.1	116
3	756.3	231	439.2	72	200.0	122	109.9	257
4	715.4	166	412.5	257	174.2	86	102.9	120
5	668.0	226	391.8	116	158.7	301	97.4	10

Table 4: Five largest values of peak horizontal velocity in the 2013 compilation. Peaks are given for original records, listed under the 25 Hz. category, and for records after application of low-pass filters with various corner frequencies. See Tables 9 to 17 to identify the accelerogram from the record number (Rec.) given here.

	Low Pass Filter Corner Frequency					
	25 Hz		10 Hz		5 Hz	
Rank	Peak, cm/s	Rec.	Peak, cm/s	Rec.	Peak, cm/s	Rec.
1	306.0	122	306.0	122	305.6	122
2	196.4	116	196.4	116	196.5	116
3	169.7	86	169.4	86	168.6	86
4	157.3	72	156.6	72	153.4	72
5	151.8	257	151.5	257	151.7	257

	Low Pass Filter Corner Frequency							
	2 Hz		1 Hz		0.5 Hz		1/3 Hz	
Rank	Peak, cm/s	Rec.	Peak, cm/s	Rec.	Peak, cm/s	Rec.	Peak, cm/s	Rec.
1	303.9	122	305.2	122	289.1	122	268.62	122
2	196.6	116	194.6	116	186.6	116	168.9	116
3	162.5	86	140.0	257	110.3	57	97.9	57
4	149.6	257	133.6	120	108.9	120	86.2	40
5	145.1	120	133.0	86	105.1	40	85.8	120

Table 5: Five largest values of peak vertical accelerations in the 2013 compilation. Peaks are given for original records, listed under the 25 Hz. category, and for records after application of low-pass filters with various corner frequencies. See Tables 9 to 17 to identify the accelerogram from the record number (Rec.) given here.

	Low Pass Filter Corner Frequency					
	25 Hz		10 Hz		5 Hz	
Rank	Peak, cm/s^2	Rec.	Peak, cm/s^2	Rec.	Peak, cm/s^2	Rec.
1	3841.5	264	1597.9	264	704.8	80
2	2318.7	31	1418.5	10	644.7	264
3	1881.9	350	1092.0	31	630.5	5
4	1773.0	10	1079.0	350	606.5	69
5	1598.0	314	1051.6	80	598.0	10

	Low Pass Filter Corner Frequency							
	2 Hz		1 Hz		0.5 Hz		1/3 Hz	
Rank	Peak, cm/s^2	Rec.	Peak, cm/s^2	Rec.	Peak, cm/s^2	Rec.	Peak, cm/s^2	Rec.
1	350.0	122	284.7	122	202.3	122	147.8	122
2	319.0	166	171.3	85	112.0	116	93.0	116
3	266.3	69	164.0	120	109.9	120	79.4	120
4	253.2	5	155.8	54	102.5	54	76.3	54
5	247.5	294	127.2	108	95.4	85	58.0	119

Table 6: Five largest values of peak vertical velocities in the 2013 compilation. Peaks are given for original records, listed under the 25 Hz. category, and for records after application of low-pass filters with various corner frequencies. See Tables 9 to 17 to identify the accelerogram from the record number (Rec.) given here.

	Low Pass Filter Corner Frequency					
	25 Hz		10 Hz		5 Hz	
Rank	Peak, cm/s	Rec.	Peak, cm/s	Rec.	Peak, cm/s	Rec.
1	195.5	122	195.3	122	195.3	122
2	137.6	116	137.3	116	137.0	116
3	79.7[1]	10[1]	76.3	54	75.8	54
4	78.8	264	71.5	264	70.6	85
5	76.5	54	70.4 [1]	5[1]	69.0	120

	Low Pass Filter Corner Frequency							
	2 Hz		1 Hz		0.5 Hz		1/3 Hz	
Rank	Peak, cm/s	Rec.	Peak, cm/s	Rec.	Peak, cm/s	Rec.	Peak, cm/s	Rec.
1	194.3	122	194.7	122	189.0	122	167.2	122
2	135.2	116	132.4	116	126.0	116	117.1	116
3	76.1	54	76.2	54	73.5	54	67.8	54
4	68.6	120	67.7	120	60.0	120	53.3[1]	297[1]
5	67.4	85	63.0	135	56.4 [1]	297[1]	53.3	120

Notes:

[1]Based on integration from acceleration, the velocity obtained from the Victoria station during the 1980 Cerro Prieto, Mexico, earthquake (Record #18, Table 9) appears at this location. It is excluded from this list because that record has data gaps, so estimates of the peak velocity values have high uncertainty (Anderson et al., 1982).

13 Appendix

Table 7: Catalog of Earthquakes contributing to the 2013 Compilation of Exceptional Ground Motions, Part 1: 1940-2000.

#	Event Name	Country	M_w	Ref#1	Nx	S	Year	Mo	Da	Hr	Mn	Sec	Lat	Long	Dep	Ref#2
1	Imperial Valley	USA, Mexico	6.95	NGAW2	1	0	1940	5	19	4	36	41	32.76	-115.416	8.8	NGAW2
2	Niigata	Japan	7.6	IRIS	1	2	1964	6	16	4	1	41	38.35	139.18	34	JMA
3	Parkfield	USA	6.19	NGAW2	1	0	1966	6	28	4	26	14	35.955	-120.498	10	NGAW2
4	San Fernando	USA	6.61	NGAW2	1	2	1971	2	9	14	0	41	34.44	-118.41	13	NGAW2
5	Gazli	Uzbekistan	6.8	NGAW2	1	2	1976	5	17	2	58	41	40.465	63.462	18.2	NGAW2
6	Tabas	Iran	7.35	NGAW2	1	2	1978	9	16	15	35	56	33.215	57.323	5.75	NGAW2
7	Imperial Valley	USA, Mexico	6.53	NGAW2	10	0	1979	10	15	23	16	54	34.644	-115.307	9.96	NGAW2
8	Victoria	Mexico	6.33	NGAW2	2	0	1980	6	9	3	28	19	32.185	-115.076	11	NGAW2
9	Westmorland	USA	5.9	NGAW2	1	0	1981	4	26	12	9	28	33.10	-115.62	2.3	NGAW2
10	Coalinga	USA	6.36	NGAW2	1	2	1983	5	2	23	42	38	36.233	-120.31	4.6	NGAW2
11	Coalinga aftershock 1	USA	5.09	NGAW2	1	2	1983	5	9	2	49	11	36.246	-120.299	12	NGAW2
12	Coalinga aftershock 2	USA	5.77	NGAW2	2	2	1983	7	22	2	39	54	36.241	-120.409	7.4	NGAW2
13	Coalinga aftershock 3	USA	5.21	NGAW2	1	2	1983	7	25	22	31	39	36.229	-120.398	8.4	NGAW2
14	Morgan Hill	USA	6.19	NGAW2	1	0	1984	4	24	21	15	18	37.306	-121.695	8.5	NGAW2
15	Valapraiso	Chile	7.9	GCMT	3	7	1985	3	3	22	47	7	-33.135	-71.871	33	PDE
16	Michoacan	Mexico	8.0	GCMT	1	7	1985	9	19	13	17	47	18.19	-102.53	27.9	PDE
17	Michoacan aftershock	Mexico	7.5	GCMT	1	7	1985	9	21	1	37	13	17.80	-101.65	30.8	PDE
18	Nahanni	Canada	6.9	NGAW2	2	2	1985	12	23	5	16	3	62.187	-124.243	8	NGAW2
19	North Palm Springs	USA	6.06	NGAW2	4	3	1986	7	8	9	20	44	34.000	-116.612	11	NGAW2
20	Whittier Narrows	USA	5.99	NGAW2	2	3	1987	10	1	14	42	20	34.049	-118.081	14.6	NGAW2
21	Superstition Hills	USA	6.7	NGAW2	2	0	1987	11	24	13	15	56	33.022	-115.831	9	NGAW2
22	Loma Prieta	USA	6.93	NGAW2	10	3	1989	10	18	0	4	15	37.041	-121.883	17.5	NGAW2
23	Manjil	Iran	7.37	NGAW2	2	0	1990	6	20	9	0	10	36.836	49.3918	16	NGAW2
24	Erzincan	Turkey	6.6	GCMT	1	0	1992	3	13	17	18	40	39.710	39.605	15	PDE*
25	Cape Mendocino	USA	7.01	NGAW2	2	2	1992	4	25	18	6	4	40.327	-124.233	9.5	NGAW2
26	Cape Mendocino aftershock	USA	6.5	GCMT	1	1	1992	4	26	7	41	40	40.415	-124.603	20.3	PDE
27	Landers	USA	7.28	NGAW2	1	0	1992	6	28	11	57	34	34.201	-116.436	7	NGAW2
28	Big Bear	USA	6.46	NGAW2	1	0	1992	6	28	15	5	36	34.210	-116.826	13	NGAW2
29	Northridge	USA	6.69	NGAW2	22	2	1994	1	17	12	30	55	34.206	-118.554	17.5	NGAW2
30	Northridge aftershock	USA	5.3	MS PDE	1	-1	1994	1	29	11	20	35	34.305	-118.579	1	PDE
31	Zanjiran	Iran	5.9	GCMT	2	0	1994	6	20	9	9	2.9	28.968	52.614	8.6	PDE
32	Kobe	Japan	6.9	NGAW2	4	0	1995	1	16	20	46	52	34.596	135.011	17.9	NGAW2
33	Miyagi-oki	Japan	5.1	MJ JMA	1	-1	1996	5	23	9	36	50	38.65	142.31	38	JMA
34	N Yamagata	Japan	5.3	PDE	1	-1	1996	8	13	2	13	3	38.80	140.58	56	JMA
35	SW Ibaraki	Japan	5.5	PDE	1	7	1996	12	21	1	28	48	36.10	139.86	53	JMA
36	E off Izu Penninsula	Japan	5.5	MJ JMA	1	0	1997	3	3	14	9	43	34.96	139.16	1	JMA
37	NE Aichi	Japan	5.6	GCMT	1	6	1997	3	16	5	51	37	34.93	137.53	39	JMA
38	NW Kagoshima	Japan	6.1	NIED	2	0	1997	3	26	8	31	48	31.969	130.361	11.8	NIED
39	NW Kagoshima	Japan	6.0	NIED	2	0	1997	5	13	5	38	28	31.945	130.305	9.24	NIED
40	Umbria Marche foreshock	Italy	5.72	NGAW2	1	1	1997	9	26	0	33	12	43.023	12.892	7	NGAW2
41	Umbria Marche	Italy	6.04	NGAW2	1	1	1997	9	26	9	40	28	43.031	12.862	6	NGAW2
42	Chamoli	India	6.6	GCMT	1	2	1999	3	28	19	5	11	30.512	79.403	15	PDE
43	Karehbas	Iran	6.2	GCMT	1	0	1999	5	6	23	0	53	29.501	51.88	17.4	PDE*
44	Kocaeli	Turkey	7.51	NGAW2	3	0	1999	8	17	0	1	40	40.748	29.99	16	NGAW2
45	Central Wakayama	Japan	5.6	NIED	1	6	1999	8	20	20	33	11	34.042	135.474	69.6	NIED
46	Chi-Chi	Taiwan	7.62	NGAW2	38	3	1999	9	20	17	47	16	23.85	120.82	8	NGAW2
47	Duzce	Turkey	7.14	NGAW2	4	0	1999	11	12	16	57	27	40.834	31.135	14	NGAW2
48	Duzce aftershock 1	Turkey	4.8	mb PDE	2	-1	1999	11	12	17	16	50	40.755	31.022	10	PDE
49	Duzce aftershock 2	Turkey	5.5	mb PDE	1	-1	1999	11	12	17	17	57	40.785	31.12	10	PDE
50	South Iceland #1	Iceland	6.5	GCMT	2	0	2000	6	17	15	40	43	63.90	-20.47	8	CENT
51	South Iceland #2	Iceland	6.4	GCMT	3	0	2000	6	21	0	51	48	63.87	-20.74	8	CENT
52	Near Niijima Island	Japan	4.2	NIED	1	0	2000	7	14	20	18	9.9	34.406	139.232	5.94	NIED
53	Yountville	USA	5.0	NGAW2	1	0	2000	9	3	8	36	30	38.379	-122.413	10.1	NGAW2
54	Tottori	Japan	6.6	GCMT	10	0	2000	10	6	4	30	18	35.275	133.350	11.3	NIED
55	Shima Penninsula Region	Japan	5.5	NIED	1	8	2000	10	30	16	42	53	34.281	136.349	43.1	NIED

Column Explanations:
MW Magnitudes are M_w unless noted otherwise.
Ref#1. Reference for M_w. NGAW2: The Next Generation Attenuwation Equation West 2 project of PEER (Ancheta et al., 2013). GCMT: Global Centroid Moment Tensor project (Ekstrom et al., 2012). NIED: National Research Institute for Earth Science and Disaster Prevention (Fukuyama et al., 1998), PDE: US Geological Survey Preliminary Determination of Epicenters, JMA: Japan Meteorological Agency.
Nx: Number of exceptional records from this earthquake.
S: Source mechanism code: 0-strike slip, 1-normal, 2-reverse, 3-oblique reverse, 4-oblique normal, 5-strike-slip in oceanic crust, 6-normal faulting in the downgoing slab in a subduction zone, 7-subduction zone thrust faulting, 8-oblique thrust faulting in a subduction zone.
Ref#2. Reference for the time and location of earthquakes. See Ref#1; CENT: USGS Centenniel Earthquake Catalog (Engdahl et al., 1998; Engdahl and Villasenor, 2002)

Table 8: Catalog of Earthquakes contributing to the 2013 Compilation of Exceptional Ground Motions, Part 2: 2001-2012.

#	Event Name	Country	M_w	Ref#1	Nx	S	Year	Mo	Da	Hr	Mn	Sec	Lat	Long	Dep	Ref#2
56	El Salvador	El Salvador	7.7	GCMT	5	6	2001	1	13	17	33	31	13.07	-88.70	38	CENT
57	Nisqually (Washington)	USA	6.8	GCMT	1	6	2001	2	28	18	54	33	47.149	-122.727	51.9	PDE
58	Geiyo	Japan	6.8	GCMT	7	6	2001	3	24	6	27	54	34.120	132.709	51.4	NIED
59	SW Ibaraki	Japan	4.9	NIED	1	7	2002	6	14	2	42	49	36.213	139.980	57	NIED
60	Changureh-Avaj	Iran	6.5	GCMT	1	2	2002	6	22	2	58	21	35.626	49.047	10	PDE
61	Denali (Alaska)	USA	7.9	NGAW2	1	0	2002	11	3	22	12	41	63.542	-147.444	8.9	NGAW2
62	Northern Miyagi	Japan	7.0	GCMT	15	7	2003	5	26	9	24	33	38.806	141.683	70.7	NIED
63	Tokachi-oki	Japan	8.3	GCMT	10	7	2003	9	25	19	50	7.6	41.780	144.078	42	NIED
64	Tokachi-oki aftershock	Japan	7.3	GCMT	1	7	2003	9	25	21	8	1.8	41.707	143.695	21.4	NIED
65	Bam	Iran	6.6	NGAW2	1	0	2003	12	26	1	56	56	28.984	58.359	6	NGAW2
66	Northern Iwate	Japan	4.1	NIED	1	2	2004	7	9	10	54	13	39.912	141.038	9.19	NIED
67	Parkfield 2004	USA	6.0	NGAW2	13	0	2004	9	28	17	15	24	35.817	-120.365	8.1	NGAW2
68	Chuetsu	Japan	6.6	GCMT	8	2	2004	10	23	8	56	0.3	37.289	138.870	13.1	NIED
69	Chuetsu aftershock 1	Japan	6.1	GCMT	1	2	2004	10	23	9	3	13	37.351	138.987	9.38	NIED
70	Chuetsu aftershock 2	Japan	5.4	PDE	1	3	2004	10	23	9	8	2.8	37.218	138.881	10.5	JMA
71	Chuetsu aftershock 3	Japan	6.3	GCMT	6	2	2004	10	23	9	34	5.7	37.303	138.933	14.2	NIED
72	Chuetsu aftershock 4	Japan	5.9	GCMT	1	2	2004	10	27	1	40	50	37.289	139.036	11.6	NIED
73	Off Nemuro Peninsula	Japan	7.0	GCMT	2	7	2004	11	28	18	32	15	42.944	145.280	48.2	NIED
74	Rumoi region	Japan	5.7	GCMT	1	2	2004	12	14	5	56	11	44.074	141.703	8.58	NIED
75	Chuetsu aftershock 5	Japan	4.5	NIED	1	2	2005	1	18	12	50	33	37.368	139.000	7.62	NIED
76	Anza	USA	5.2	GCMT	1	0	2005	6	12	15	41	46	33.533	-116.578	14.1	GCMT
77	Miyagi-oki	Japan	7.2	GCMT	3	7	2005	8	16	2	46	26	38.151	142.280	41.6	NIED
78	Noto Hanto	Japan	6.7	GCMT	4	3	2007	3	25	0	41	58	37.221	136.686	10.7	NIED
79	Northern Mie	Japan	5.1	GCMT	2	2	2007	4	15	3	19	30	34.791	136.408	16	NIED
80	NE Ehime	Japan	5.1	GCMT	1	5	2007	4	26	0	2	57	33.889	133.585	39.1	NIED
81	Chuetsu-oki	Japan	6.6	GCMT	2	2	2007	7	16	1	13	23	37.557	138.609	16.8	NGAW2
82	Mogul, Nevada	USA	5.0	GCMT	3	0	2008	4	26	6	40	11	39.522	-119.923	3.1	GCMT
83	Iwate-Miyagi Nairiku	Japan	6.9	GCMT	6	2	2008	6	13	23	43	45	39.03	140.881	7.77	NGAW2
84	Southern Iwate aftershock	Japan	5.5	JMA	1	2	2008	6	14	0	18	14	39.14	140.93	10	JMA
85	Southern Iwate aftershock	Japan	4.8	GCMT	1	2	2008	6	14	14	42	32	38.995	140.890	9.99	NIED
86	Soutnern Iwate aftershock	Japan	5.1	GCMT	1	2	2008	6	16	14	14	38	38.997	140.841	10.8	NIED
87	Northern Iwate	Japan	6.8	GCMT	9	2	2008	7	23	15	26	20	39.732	141.635	108	NIED
88	l^Aquila	Italy	6.31	NGAW2	3	1	2009	4	6	1	32	39	42.548	13.380	9.5	NGAW2
89	Suruga Bay	Japan	6.2	NIED	2	2	2009	8	10	20	7	9	34.786	138.499	23.3	NIED
90	Off Izu Peninsula #1	Japan	4.9	GCMT	1	0	2009	12	17	14	45	25	34.959	139.137	4	NIED
91	Off Izu Peninsula #2	Japan	5.0	GCMT	1	0	2009	12	17	23	45	37	34.961	139.129	4.9	JMA
92	Maule	Chile	8.78	GCMT	9	7	2010	2	27	6	34	14	-35.91	-72.73	35	GCMT
93	El Mayor - Cucapah	Mexico, USA	7.19	NGAW2	2	0	2010	4	4	22	40	42	32.300	-115.267	5.5	NGAW2
94	Canterbury (Darfield)	New Zealand	6.97	NGAW2	9	0	2010	9	3	16	35	42	-43.615	172.049	10.9	NGAW2
95	Christchurch	New Zealand	6.2	NGAW2	10	3	2011	2	21	23	51	42	-43.571	172.703	6	NGAW2
96	Northern Gifu	Japan	4.8	NIED	1	3	2011	2	26	17	18	59	36.158	137.458	3.84	NIED
97	Tohoku	Japan	9.1	GCMT	78	7	2011	3	11	5	46	18	38.103	142.861	23.7	NIED
98	E off Fukushima #1	Japan	6.1	MJ JMA	1	-1	2011	3	11	5	54	31	37.51	141.35	34	JMA
99	Far E off Ibaraki	Japan	7.9	GCMT	3	7	2011	3	11	6	15	34	36.108	141.265	43.2	NIED
100	E off Fukushima #2	Japan	6.1	MJ JMA	1	-1	2011	3	11	8	41	55	37.42	141.27	30	JMA
101	Mid Niigata	Japan	6.3	GCMT	1	2	2011	3	11	18	59	16	36.986	138.598	8.38	NIED
102	Fuji Region	Japan	6.0	GCMT	1	0	2011	3	15	13	31	46	35.309	138.714	14.3	NIED
103	Northern Ibaraki #1	Japan	5.8	GCMT	4	1	2011	3	19	9	56	48	36.784	140.571	5.37	NIED
104	E off Miyagi	Japan	7.1	GCMT	22	7	2011	4	7	14	32	43	38.203	141.924	65.7	NIED
105	Fukushima Hamadori	Japan	6.7	GCMT	8	1	2011	4	11	8	16	12	36.946	140.673	6.42	NIED
106	Eastern Fukushima	Japan	5.9	GCMT	2	3	2011	4	12	5	7	42	37.053	140.643	15.1	NIED
107	Northern Ibaraki #2	Japan	4.9	NIED	1	1	2011	4	13	22	35	50	36.778	140.573	8.77	NIED
108	Central Wakayama	Japan	5.0	GCMT	1	2	2011	7	5	10	18	43	36.990	135.234	7.33	NIED
109	Central Wakayama	Japan	4.3	NIED	1	2	2011	7	5	10	34	56	36.996	135.242	7.08	NIED
110	Northern Ibaraki #3	Japan	5.1	GCMT	1	1	2011	9	21	13	30	57	36.737	140.577	8.64	NIED
111	Northern Ibaraki #4	Japan	4.0	NIED	1	1	2011	11	4	15	45	10	36.782	140.550	8.39	NIED
112	Northern Ibaraki #5	Japan	5.0	GCMT	1	1	2011	11	20	1	23	41	36.711	140.588	8.99	NIED
113	Northern Ibaraki #6	Japan	5.2	GCMT	1	1	2012	3	9	17	25	31	36.718	140.613	6.52	NIED

Column Explanations: See explanations in Table 7

Table 9: Exceptional Ground Motion Records, Part 1, 1940-1992

Rec#	Station	EQ#	Eq name	M_w	A_H	V_H
1	El Centro	1	Imperial Valley	7.0	346.9	60.8
2	Kawagishi-cho	2	Niigata	7.6	209.4	74.8
3	Cholome 2wa	3	Parkfield	6.2	466.3	74.9
4	Pacoima Dam	4	San Fernando	6.6	1356	123
5	Karakyr	5	Gazli	6.8	756.7	62.1
6	Tabas	6	Tabas	7.3	953.6	36.2
7	Agrarias	7	Imperial Valley	6.5	378.6	45.9
8	El Centro Array #4	7	Imperial Valley	6.5	537.4	77
9	El Centro Array #5	7	Imperial Valley	6.5	560.8	88
10	El Centro Array #6	7	Imperial Valley	6.5	478.6	111
11	El Centro Array #7	7	Imperial Valley	6.5	544.7	85.4
12	Differential Array	7	Imperial Valley	6.5	503.5	72.1
13	Bonds Corner	7	Imperial Valley	6.5	772	53
14	El Centro Array #8	7	Imperial Valley	6.5	627.8	72.4
15	EC Meloland Overpass	7	Imperial Valley	6.5	434.2	103
16	Westmorland	7	Imperial Valley	6.5	121.1	23.6
17	Cerro Prieto	8	Victoria	6.3	626.8	37
18	Victoria	8	Victoria	6.3	1087	90
19	Westmorland	9	Westmorland	5.9	475	55
20	Pleasant Valley P.P.	10	Coalinga	6.4	604.9	73.7
21	Anticline Ridge	11	Coalinga aftershock 1	5.1	298.3	24.3
22	Oil City	12	Coalinga aftershock 2	5.8	928	44.3
23	Transmitter Hill	12	Coalinga aftershock 2	5.8	1188	65.7
24	Old Chp	13	Coalinga aftershock 3	5.2	719	35.2
25	Coyote Lake Dam	14	Morgan Hill	6.2	1191	77.1
26	Llolleo	15	Valapraiso	7.9	729.8	43
27	Melipilla	15	Valapraiso	7.9	674.7	40.4
28	San Isidro	15	Valapraiso	7.9	798.8	45.2
29	SCT	16	Michoacan	8.0	173.2	63.9
30	Paraiso	17	Michoacan aftershock	7.5	736.1	12.4
31	Site 1	18	Nahanni	6.9	1332	46.8
32	Site 2	18	Nahanni	6.9	575.1	37.5
33	Devers Substation	19	North Palm Springs	6.1	1198	104
34	Desert Hot Springs	19	North Palm Springs	6.1	365.6	33.5
35	North Palm Springs P	19	North Palm Springs	6.1	767	73.8
36	Whitewater Canyon -	19	North Palm Springs	6.1	686.3	35.9
37	Whittier Narrows Dam	20	Whittier Narrows	6.0	305.9	15.9
38	Tarzana	20	Whittier Narrows	6.0	634.5	30.9
39	Parachute Test Site	21	Superstition Hills	6.7	556.3	115
40	Superstition Mtn. Ca	21	Superstition Hills	6.7	206.6	121
41	BRAN	22	Loma Prieta	6.9	646.4	56.4
42	Capitola	22	Loma Prieta	6.9	541.6	40.8
43	Corralitos	22	Loma Prieta	6.9	634.1	56.5
44	Los Gatos Lexington	22	Loma Prieta	6.9	453.9	119
45	Gilroy Array #3	22	Loma Prieta	6.9	532.7	24.8
46	Hollister South Pine	22	Loma Prieta	6.9	364.9	63.1
47	LGPC	22	Loma Prieta	6.9	888.4	118
48	Redwood Highway	22	Loma Prieta	6.9	273.1	56.9
49	WAHO	22	Loma Prieta	6.9	665.9	35.2
50	Saratoga	22	Loma Prieta	6.9	408.2	74.7
51	Abbar	23	Manjil	7.4	675.5	87.1
52	Abhar	23	Manjil	7.4	219.6	52.9
53	Erzincan	24	Erzincan	6.6	517.9	95.5
54	Cape Mendocino, Petr	25	Cape Mendocino	7.0	1720	135
55	Petrolia Gen Store 1	25	Cape Mendocino	7.0	695.7	98.5
56	Petrolia Gen Store 2	26	Cape Mendocino aftershock	6.5	589	61.3
57	Lucerne	27	Landers	7.3	807.5	147
58	Big Bear Lake	28	Big Bear	6.5	633.4	34.9

Table 10: Exceptional Ground Motion Records, Part 2, 1994-1997

r#	Station	EQ#	Eq name	M_w	A_H	V_H
59	Arleta Fire Station	29	Northridge	6.7	359.3	39.8
60	Beverly Hills 12520	29	Northridge	6.7	676.8	38.8
61	Canoga Park	29	Northridge	6.7	389.6	64.2
62	Castaic Old Ridge Ro	29	Northridge	6.7	559.4	57.6
63	Sylmar County Hospit	29	Northridge	6.7	827.4	131
64	Jensen F.P. Generato	29	Northridge	6.7	1096	98.1
65	Jensen F.P. Administ	29	Northridge	6.7	621.5	117
66	LA Dam	29	Northridge	6.7	328.7	74.9
67	14145 Mullholand Dr.	29	Northridge	6.7	494.1	87.6
68	Newhall F.S.	29	Northridge	6.7	731.8	119
69	Pacoima Dam	29	Northridge	6.7	1560	107
70	Pardee	29	Northridge	6.7	695.5	75.5
71	West Pico Canyon Roa	29	Northridge	6.7	411.3	118
72	Rinaldi Receiving St	29	Northridge	6.7	863.8	157
73	Santa Monica City Ha	29	Northridge	6.7	866.3	41
74	17645 Saticoy St., N	29	Northridge	6.7	461.3	62.7
75	Sylmar Converter Stn	29	Northridge	6.7	775.1	135
76	Sepulvelda VA Hospit	29	Northridge	6.7	949.5	80.1
77	Simi Valley	29	Northridge	6.7	795.9	68.1
78	Sylmar Valve Hall Fl	29	Northridge	6.7	871.8	122
79	Sylmar Converter Stn	29	Northridge	6.7	614.9	124
80	Tarzana	29	Northridge	6.7	1965	110
81	Brown's Canyon	30	Northridge aftershock	5.3	774.2	38.5
82	Maymand	31	Zanjiran	5.9	531.9	25.9
83	Zanjiran	31	Zanjiran	5.9	1053	42.6
84	KJMA	32	Kobe	6.9	837.6	95.7
85	Port Island, Kobe	32	Kobe	6.9	377.2	85.4
86	Takatori	32	Kobe	6.9	688.1	170
87	Takarazuka	32	Kobe	6.9	745.5	89.5
88	MYG011 Oshika	33	Miyagi-oki	5.1	571.6	16.8
89	MYG005 Naruko	34	N Yamagata	5.3	718.7	10.8
90	TCG009 Imaichi	35	SW Ibaraki	5.5	524.3	23.2
91	SZO002 Itoh	36	E off Izu Penninsula	5.5	616.9	32.5
92	AIC010 Tsukude	37	NE Aichi	5.6	597.7	16.7
93	KGS002 Izumi	38	NW Kagoshima	6.1	903.3	16.6
94	KGS005 Miyanojoh	38	NW Kagoshima	6.1	527.3	37.4
95	KGS002 Izumi	39	NW Kagoshima	6.0	762.5	23
96	KGS005 Miyanojoh	39	NW Kagoshima	6.0	957.9	47.4
97	0593 Nocera Umbra	40	Umbria Marche foreshock	5.7	554.1	20.8
98	0594 Nocera Umbra	41	Umbria Marche	6.0	717.2	34.5

cc

Table 11: Exceptional Ground Motion Records, Part 3, 1999

r#	Station	EQ#	Eq name	M_w	A_H	V_H
99	Gopeshwar	42	Chamoli	6.6	366.4	50.7
100	Balaadeh	43	Karehbas	6.2	458.6	18.9
101	Duzce	44	Kocaeli	7.5	362.5	54.6
102	Sakarya	44	Kocaeli	7.5	374	68.5
103	Yarimca	44	Kocaeli	7.5	376.5	80.5
104	WKY005	45	Central Wakayama	5.6	583.7	10.9
105	CHY006	46	Chi-Chi	7.6	385	66.7
106	CHY024	46	Chi-Chi	7.6	307.6	63.2
107	CHY028	46	Chi-Chi	7.6	805.2	78.3
108	CHY080	46	Chi-Chi	7.6	1187	128
109	CHY101	46	Chi-Chi	7.6	498.7	109
110	CHY104	46	Chi-Chi	7.6	200.7	58.6
111	NSY	46	Chi-Chi	7.6	143.8	60
112	TCU036	46	Chi-Chi	7.6	137.4	65.5
113	TCU039	46	Chi-Chi	7.6	218.3	68
114	TCU040	46	Chi-Chi	7.6	160.2	57.5
115	TCU049	46	Chi-Chi	7.6	319.6	63
116	TCU052	46	Chi-Chi	7.6	502.1	196
117	TCU055	46	Chi-Chi	7.6	284.9	58.8
118	TCU059	46	Chi-Chi	7.6	176.5	64.1
119	TCU063	46	Chi-Chi	7.6	189.6	85.7
120	TCU065	46	Chi-Chi	7.6	789.4	144
121	TCU067	46	Chi-Chi	7.6	557	93.3
122	TCU068	46	Chi-Chi	7.6	526.8	306
123	TCU070	46	Chi-Chi	7.6	249	60.4
124	TCU071	46	Chi-Chi	7.6	796	71.3
125	TCU072	46	Chi-Chi	7.6	466.9	72.4
126	TCU074	46	Chi-Chi	7.6	608	79
127	TCU075	46	Chi-Chi	7.6	325.7	105
128	TCU076	46	Chi-Chi	7.6	421.3	79.3
129	TCU079	46	Chi-Chi	7.6	908	50.1
130	TCU082	46	Chi-Chi	7.6	260.3	62.8
131	TCU084	46	Chi-Chi	7.6	1031	124
132	TCU087	46	Chi-Chi	7.6	121.9	50.7
133	TCU095	46	Chi-Chi	7.6	680.9	49.2
134	TCU101	46	Chi-Chi	7.6	266.1	76.2
135	TCU102	46	Chi-Chi	7.6	298.8	112
136	TCU103	46	Chi-Chi	7.6	168	68.7
137	TCU109	46	Chi-Chi	7.6	202.3	61.3
138	TCU117	46	Chi-Chi	7.6	136.6	62
139	TCU128	46	Chi-Chi	7.6	194.5	77.7
140	TCU129	46	Chi-Chi	7.6	1002	69.7
141	WGK	46	Chi-Chi	7.6	492	81.1
142	WNT	46	Chi-Chi	7.6	945.9	64.6
143	Bolu	47	Duzce	7.1	901.2	62.6
144	Duzce	47	Duzce	7.1	513.1	86.8
145	IRIGM 496	47	Duzce	7.1	1067	50.8
146	Lamont 375	47	Duzce	7.1	971.7	35.7
147	IRIGM 492	48	Duzce aftershock 1	4.8	615.7	26.8
148	IRIGM 496	48	Duzce aftershock 1	4.8	1071	37.6
149	IRIGM 496	49	Duzce aftershock 2	5.5	806.8	33.9

cc

Table 12: Exceptional Ground Motion Records, Part 4, 2000-2003

r#	Station	EQ#	Eq name	M_w	A_H	V_H	
150	004674 Flagbjarnarho	50	South Iceland #1	6.5	391.9	63.4	
151	006263 Kaldarholt	50	South Iceland #1	6.5	850.3	43.6	
152	006332 Thjorsartun	51	South Iceland #2	6.4	704	83.6	
153	006334 Solheimar	51	South Iceland #2	6.4	719.6	106	
154	006349 Thjorsarbru	51	South Iceland #2	6.4	822	102	
155	TKY010 Niijima	52	Near Niijima Island	4.2	551.7	12.3	
156	Napa	53	Yountville	5.0	630.5	44.3	
157	HRS001 Takano	54	Tottori	6.6	487	12.2	
158	HRS002 Tohjoh	54	Tottori	6.6	573.7	8.66	
159	HRS005 Yuki	54	Tottori	6.6	538.6	14.3	
160	OKY004 Niimi	54	Tottori	6.6	875.2	26.3	
161	SMN003 Yokota	54	Tottori	6.6	506.7	14	
162	SMNH01 Hakuta	54	Tottori	6.6	837.6	43.3	
163	SMNH02 Nita	54	Tottori	6.6	582.5	29.6	
164	TTR007 Kohfu	54	Tottori	6.6	797.8	42.4	
165	TTR009 Nichinan	54	Tottori	6.6	738.8	41.6	
166	TTRH02 Hino	54	Tottori	6.6	1070	125	
167	MIEH05 Owase	55	Shima Penninsula Region	5.5	542.4	13	
168	Puerto La Libertad,	56	El Salvador	7.7	1196	55.3	
169	San Pedro Nonualco,	56	El Salvador	7.7	600.4	39.3	
170	Santa Tecla	56	El Salvador	7.7	866.9	60.4	
171	Santiago de Maria	56	El Salvador	7.7	866.1	40.7	
172	Armenia, Sonsonate	56	El Salvador	7.7	608.5	63.6	
173	Seattle	57	Nisqually (Washington)	6.8	703.2	41.5	
174	EHM003 Tohyo	58	Geiyo	6.8	504.2	32.8	
175	HRS009 Yuki	58	Geiyo	6.8	849.9	31.1	
176	HRS017 Mihara	58	Geiyo	6.8	695.1	12.5	
177	HRS019 Kure	58	Geiyo	6.8	527	24.4	
178	HRSH01 MIHARA	58	Geiyo	6.8	638.5	18.9	
179	Mistugi	58	Geiyo	6.8	558.1	19.4	
180	EHMH05 Tobe	58	Geiyo	6.8	609.9	17.2	
181	IBR013 Hokota	59	SW Ibaraki	4.9	594.5	16.1	
182	Avaj	60	Changureh-Avaj	6.5	517	24	
183	Taps Pump Station #1	61	Denali (Alaska)	7.9	388.5	103	
184	IWTH05 Fujisawa	62	Northern Miyagi	7.0	599.8	16.4	
185	IWTH26 Ichinoseki-E	62	Northern Miyagi	7.0	538.5	26.8	
186	IWT007 Kamaishi	62	Northern Miyagi	7.0	1048	25.1	
187	IWT012 Kitakami	62	Northern Miyagi	7.0	526	32.7	
188	IWTH23 Kamaishi	62	Northern Miyagi	7.0	554.7	17.5	
189	MYGH03 Karakuwa	62	Northern Miyagi	7.0	821.5	14.4	
190	MYG002 Utatsu	62	Northern Miyagi	7.0	926.1	22.8	
191	MYG003 Tohwa	62	Northern Miyagi	7.0	575.4	11.8	
192	MYG011 Oshika	62	Northern Miyagi	7.0	1581	59	
193	MYGH05 Onoda	62	Northern Miyagi	7.0	634.9	32.2	
194	IWTH27 Rikuzentakata	62	Northern Miyagi	7.0	911	16.9	
195	IWTH04 Sumita	62	Northern Miyagi	7.0	864.4	37.4	
196	IWTH02 Tamayama	62	Northern Miyagi	7.0	802.7	19.6	
197	MYGH04 Touwa	62	Northern Miyagi	7.0	669.1	19	
198	IWTH21 Yamada	62	Northern Miyagi	7.0	679.4	20.5	
199	KSRH10 Hamanaka	63	Tokachi-oki	8.3	590.7	39.6	
200	HKD100 Hiroo	63	Tokachi-oki	8.3	973.5	52.1	
201	HKD066 Shibetsu	63	Tokachi-oki	8.3	563.8	77.5	
202	HKD075 Hamanaka	63	Tokachi-oki	8.3	542.5	31	
203	HKD086 Chokubetsu	63	Tokachi-oki	8.3	807.5	80.9	
204	HKD092 Ikeda	63	Tokachi-oki	8.3	676.2	55.4	
205	KSRH07 Tsurui-S	63	Tokachi-oki	8.3	523	42.4	
206	NMRH02 Shibetsu S	63	Tokachi-oki	8.3	542.7	28.5	
207	KSRH03 Shibecha	63	Tokachi-oki	8.3	307.2	29.4	
208	HKD129	63	Tokachi-oki	8.3	90.68	31.7	
209	HKD109 Urakawa	64	Tokachi-oki aftershock	7.3	660.9	51.2	
210	Bam	65	Bam	6.6	865.3	120	cc

Table 13: Exceptional Ground Motion Records, Part 5, 2004-2008

r#	Station	EQ#	Eq name	M_w	A_H	V_H
211	IWT021	66	Northern Iwate	4.1	597.2	15.9
212	CHOLAME 2WA	67	Parkfield 2004	6.0	598.3	63.4
213	Cholame 3E	67	Parkfield 2004	6.0	734.6	34.6
214	Cholame 3W	67	Parkfield 2004	6.0	559.2	45.2
215	Cholame 4W	67	Parkfield 2004	6.0	573.9	38.2
216	Stone Corral 1E	67	Parkfield 2004	6.0	893.6	43.5
217	Fault Zone 11	67	Parkfield 2004	6.0	929.1	27.7
218	Fault Zone 8	67	Parkfield 2004	6.0	539.2	23.5
219	Fault Zone 1	67	Parkfield 2004	6.0	861	82.2
220	Fault Zone 14	67	Parkfield 2004	6.0	1287	88.1
221	Gold Hill 3W	67	Parkfield 2004	6.0	708.5	25.6
222	Joaquin Canyon	67	Parkfield 2004	6.0	779.6	32.8
223	Slack Canyon	67	Parkfield 2004	6.0	344.2	53.2
224	Vinyard Canyon 2W	67	Parkfield 2004	6.0	603.4	31.3
225	NIGH11 Kawanishi	68	Chuetsu	6.6	639.9	68.5
226	Kawaguchi	68	Chuetsu	6.6	1788	137
227	NIG020 Koide	68	Chuetsu	6.6	637.1	39.4
228	NIG028 Nagaoka-Shish	68	Chuetsu	6.6	903	66.8
229	NIG017 Nagaoka	68	Chuetsu	6.6	561.7	42.2
230	NIGH01 NAGAOKA	68	Chuetsu	6.6	854.4	69
231	NIG019 Ojiya	68	Chuetsu	6.6	1521	136
232	NIG021 Tohkamachi	68	Chuetsu	6.6	1762	73.5
233	NIGH01 Nagaoka	69	Chuetsu aftershock 1	6.1	796.3	41.9
234	NIG019 Ojiya	70	Chuetsu aftershock 2	5.4	503.8	21.6
235	NIG020 Koide	71	Chuetsu aftershock 3	6.3	735.4	41.1
236	NIG019 Ojiya	71	Chuetsu aftershock 3	6.3	826	71.4
237	NIG021 Tohkamachi	71	Chuetsu aftershock 3	6.3	974.7	57.5
238	NIG024 Yasuduka	71	Chuetsu aftershock 3	6.3	519	24
239	NIGH11 Kawanishi	71	Chuetsu aftershock 3	6.3	761.5	47.3
240	NIGH12 Yunotani	71	Chuetsu aftershock 3	6.3	564.6	28.7
241	NIG020 Koide	72	Chuetsu aftershock 4	5.9	541.9	39.6
242	HKD074 Nosappu	73	Off Nemuro Peninsula	7.0	582.9	29.1
243	KSRH06 TSURUI-E	73	Off Nemuro Peninsula	7.0	787.9	31.3
244	Minatomachi	74	Rumoi region	5.7	1206	70.9
245	NIG028 Nagaoka-Shish	75	Chuetsu aftershock 5	4.5	554	19.9
246	Santa Rosa	76	Anza	5.2	959.9	17.3
247	MYG002	77	Miyagi-oki	7.2	547.8	17.2
248	MYG004	77	Miyagi-oki	7.2	563.9	19
249	MYG011	77	Miyagi-oki	7.2	531.7	19.2
250	ISK003	78	Noto Hanto	6.7	536.6	41.4
251	ISK004	78	Noto Hanto	6.7	662	26.1
252	ISK005	78	Noto Hanto	6.7	938	102
253	ISK006	78	Noto Hanto	6.7	963.7	56
254	MIE004	79	Northern Mie	5.1	778.7	35.2
255	MIEH10 GEINOU	79	Northern Mie	5.1	861.2	27.5
256	KOC008	80	NE Ehime	5.1	536.6	7.53
257	NIG018 Kashiwazaki	81	Chuetsu-oki	6.6	845.1	152
258	NIG019 Ojiya	81	Chuetsu-oki	6.6	507.6	52.8
259	MOGL	82	Mogul, Nevada	5.0	1114	52.8
260	MOGE	82	Mogul, Nevada	5.0	843.6	23
261	HONJ	82	Mogul, Nevada	5.0	640.2	19.4
262	AKTH04 Higashinaruse	83	Iwate-Miyagi Nairiku	6.9	2504	75.3
263	IWTH24 Kanegasaki	83	Iwate-Miyagi Nairiku	6.9	533.9	35.7
264	IWTH25 Ichinoseki_W	83	Iwate-Miyagi Nairiku	6.9	1444	69.2
265	IWTH26 Ichinoseki-E	83	Iwate-Miyagi Nairiku	6.9	1168	58.7
266	MYG004 Tsukidate	83	Iwate-Miyagi Nairiku	6.9	797.2	51.9
267	MYG005 Naruko	83	Iwate-Miyagi Nairiku	6.9	525.2	79.2
268	IWTH25 Ichinoseki_W	84	Southern Iwate aftershock	5.5	787.5	21.1
269	IWTH25 Ichinoseki_W	85	Southern Iwate aftershock	4.8	941.7	20.4
270	IWTH25 Ichinoseki_W	86	Soutnern Iwate aftershock	5.1	726.9	20
271	AOM012 Hachinone	87	Northern Iwate	6.8	614.7	28.7
272	IWT001 Taneichi	87	Northern Iwate	6.8	855.9	32.5
273	IWT007 Kamaishi	87	Northern Iwate	6.8	546.2	20.2
274	IWT021 Nishine	87	Northern Iwate	6.8	512.5	22.9
275	IWTH02 Tamayama	87	Northern Iwate	6.8	1023	26.1
276	IWTH03 Iwaizume	87	Northern Iwate	6.8	635.1	16.9
277	IWTH09 Kuji_S	87	Northern Iwate	6.8	527.6	15
278	IWTH12 Kunohe	87	Northern Iwate	6.8	904.3	31.3
279	MYG002 Utatsu	87	Northern Iwate	6.8	543.3	10
280	ITAQA	88	l^Aquila	6.3	440.9	32.6
281	ITAQG	88	l^Aquila	6.3	504.4	39.3
282	ITAQV	88	l^Aquila	6.3	756.5	47

cc

Table 14: Exceptional Ground Motion Records, Part 6, 2009-Feb. 2011

r#	Station	EQ#	Eq name	M_w	A_H	V_H
283	SZOH39 Nishiizu	89	Suruga Bay	6.2	533.8	24.5
284	SZOH33	89	Suruga Bay	6.2	537.9	22.3
285	SZO002	90	Off Izu Peninsula #1	4.9	488.1	37.5
286	SZO002	91	Off Izu Peninsula #2	5.0	672.8	48.8
287	Constitucion	92	Maule	8.8	705	74.2
288	Concepcion	92	Maule	8.8	393.4	67.7
289	Talca	92	Maule	8.8	499.3	34.3
290	Hualane	92	Maule	8.8	520	39.3
291	Curico	92	Maule	8.8	491.6	34
292	Angol	92	Maule	8.8	685.3	37.6
293	Llolleo	92	Maule	8.8	568.5	35.8
294	Santiago Maipu	92	Maule	8.8	504.5	40.5
295	Vina Del Mar - El Sa	92	Maule	8.8	438.1	58
296	CE01711	93	El Mayor - Cucapah	7.2	380.5	45.1
297	NP00931	93	El Mayor - Cucapah	7.2	333.5	67.9
298	NZCCCC	94	Canterbury (Darfield)	7.0	237.4	60.5
299	NZCHHC	94	Canterbury (Darfield)	7.0	194.3	50.8
300	NZDFHS	94	Canterbury (Darfield)	7.0	489.1	37.1
301	NZGDLC	94	Canterbury (Darfield)	7.0	828	113
302	NZHORC	94	Canterbury (Darfield)	7.0	517.7	84.8
303	NZHVSC	94	Canterbury (Darfield)	7.0	652	31.4
304	NZLINC	94	Canterbury (Darfield)	7.0	503	83.1
305	NZROLC	94	Canterbury (Darfield)	7.0	416.9	64.7
306	NZTPLC	94	Canterbury (Darfield)	7.0	292.1	31.5
307	NZCBGS	95	Christchurch	6.2	630.6	77
308	NZCCCC	95	Christchurch	6.2	475.9	71.4
309	NZCHHC	95	Christchurch	6.2	448.3	85
310	NZCMHS	95	Christchurch	6.2	407.2	48.3
311	NZHPSC	95	Christchurch	6.2	248.4	37.8
312	NZHVSC	95	Christchurch	6.2	1310	97.3
313	NZLPCC	95	Christchurch	6.2	980.4	47.6
314	NZPRPC	95	Christchurch	6.2	710.6	109
315	NZREHS	95	Christchurch	6.2	718	92
316	NZSHLC	95	Christchurch	6.2	335.5	70.3
317	GIF007	96	Northern Gifu	4.8	1549	40.4

cc

Table 15: Exceptional Ground Motion Records, Part 7, March 2011 (Tohoku K-NET records)

r#	Station	EQ#	Eq name	M_w	A_H	V_H
318	CHB007	97	Tohoku	9.1	1048	33.6
319	FKS001	97	Tohoku	9.1	672.6	51.3
320	FKS002	97	Tohoku	9.1	624.8	35.8
321	FKS004	97	Tohoku	9.1	692.5	24.8
322	FKS005	97	Tohoku	9.1	752.2	51.4
323	FKS006	97	Tohoku	9.1	632.8	48.1
324	FKS008	97	Tohoku	9.1	1067	43.4
325	FKS009	97	Tohoku	9.1	803.3	50.1
326	FKS010	97	Tohoku	9.1	1193	59.3
327	FKS012	97	Tohoku	9.1	339.6	54.6
328	FKS016	97	Tohoku	9.1	1420	60.2
329	FKS017	97	Tohoku	9.1	698	65
330	FKS018	97	Tohoku	9.1	1077	50.4
331	FKS024	97	Tohoku	9.1	391.4	57.3
332	IBR002	97	Tohoku	9.1	605.3	52.4
333	IBR003	97	Tohoku	9.1	1859	70.9
334	IBR004	97	Tohoku	9.1	1304	48.7
335	IBR005	97	Tohoku	9.1	980.1	64.2
336	IBR006	97	Tohoku	9.1	855.9	43
337	IBR007	97	Tohoku	9.1	545.5	51.3
338	IBR013	97	Tohoku	9.1	1638	72
339	IBR014	97	Tohoku	9.1	523.6	40.4
340	IBR016	97	Tohoku	9.1	516.2	25.6
341	IBR017	97	Tohoku	9.1	515.6	25.4
342	IBR018	97	Tohoku	9.1	662.3	41.5
343	IWT007	97	Tohoku	9.1	724.8	32
344	IWT009	97	Tohoku	9.1	572.3	21.8
345	IWT010	97	Tohoku	9.1	1180	59.8
346	IWT012	97	Tohoku	9.1	623.1	54.3
347	KNG206	97	Tohoku	9.1	369.5	68.2
348	MYG002	97	Tohoku	9.1	768.9	29.2
349	MYG003	97	Tohoku	9.1	877	32.8
350	MYG004	97	Tohoku	9.1	2761	117
351	MYG006	97	Tohoku	9.1	548.6	89.1
352	MYG007	97	Tohoku	9.1	698.2	41.4
353	MYG009	97	Tohoku	9.1	542.5	46.4
354	MYG010	97	Tohoku	9.1	490.9	62
355	MYG011	97	Tohoku	9.1	926.3	36.3
356	MYG012	97	Tohoku	9.1	1985	63.3
357	MYG013	97	Tohoku	9.1	1817	90.3
358	MYG014	97	Tohoku	9.1	530.6	29.8
359	MYG015	97	Tohoku	9.1	433.7	70
360	MYG016	97	Tohoku	9.1	406.5	53.9
361	MYG017	97	Tohoku	9.1	368.1	58.2
362	TCG006	97	Tohoku	9.1	395.2	70.2
363	TCG009	97	Tohoku	9.1	1438	48.5
364	TCG014	97	Tohoku	9.1	1274	64

Table 16: Exceptional Ground Motion Records, Part 8, March 2011 (Tohoku KiK-net records and March aftershocks)

r#	Station	EQ#	Eq name	M_w	A_H	V_H
365	AKTH04	97	Tohoku	9.1	580.4	19.7
366	FKSH09	97	Tohoku	9.1	550.3	26.1
367	FKSH10	97	Tohoku	9.1	1080	35.9
368	FKSH11	97	Tohoku	9.1	504.7	55.8
369	FKSH12	97	Tohoku	9.1	441.3	40.5
370	FKSH14	97	Tohoku	9.1	469.8	87.2
371	FKSH18	97	Tohoku	9.1	611	40.7
372	FKSH19	97	Tohoku	9.1	872.1	67.2
373	IBRH07	97	Tohoku	9.1	197.6	60.2
374	IBRH11	97	Tohoku	9.1	962.9	62.2
375	IBRH12	97	Tohoku	9.1	688.9	36.3
376	IBRH13	97	Tohoku	9.1	559.3	36.9
377	IBRH15	97	Tohoku	9.1	990.3	34.8
378	IBRH16	97	Tohoku	9.1	655.8	34.8
379	IBRH17	97	Tohoku	9.1	500.2	25.7
380	IBRH18	97	Tohoku	9.1	637.1	33.5
381	IWTH02	97	Tohoku	9.1	707	21
382	IWTH04	97	Tohoku	9.1	427.7	23.9
383	IWTH05	97	Tohoku	9.1	767.5	34.6
384	IWTH23	97	Tohoku	9.1	489.4	17.9
385	IWTH26	97	Tohoku	9.1	584.4	34.7
386	IWTH27	97	Tohoku	9.1	860.9	20.8
387	MYGH03	97	Tohoku	9.1	494.4	17.8
388	MYGH04	97	Tohoku	9.1	576.5	31.1
389	MYGH05	97	Tohoku	9.1	496.1	49.7
390	MYGH10	97	Tohoku	9.1	1026	62.6
391	MYGH12	97	Tohoku	9.1	558.6	34.6
392	TCGH10	97	Tohoku	9.1	674	45.1
393	TCGH12	97	Tohoku	9.1	483	41.7
394	TCGH13	97	Tohoku	9.1	920	64.7
395	TCGH16	97	Tohoku	9.1	1233	79.5
396	IBRH13	98	E off Fukushima #1	6.1	787.6	50.3
397	IBR003	99	Far E off Ibaraki	7.9	579.9	18.8
398	IBR013	99	Far E off Ibaraki	7.9	938	45.3
399	IBRH18	99	Far E off Ibaraki	7.9	624.1	28.9
400	FKS010	100	E off Fukushima #2	6.1	768.7	25.7
401	NIG023	101	Mid Niigata	6.3	771.5	32.7
402	SZO011	102	Fuji Region	6	1033	79.8
403	IBR003	103	Northern Ibaraki #1	5.8	592.5	16.9
404	IBR004	103	Northern Ibaraki #1	5.8	576.3	16.4
405	IBRH13	103	Northern Ibaraki #1	5.8	1058	67.1
406	IBRH14	103	Northern Ibaraki #1	5.8	537.2	11.7

Table 17: Exceptional Ground Motion Records, Part 9, April 2011-Jan 2012

407	FKS001	104	E off Miyagi	7.1	582.7	18.9
408	FKS004	104	E off Miyagi	7.1	513.3	13
409	IWT007	104	E off Miyagi	7.1	746.5	35
410	IWT009	104	E off Miyagi	7.1	674.7	31.7
411	IWT010	104	E off Miyagi	7.1	844.7	58.4
412	IWT012	104	E off Miyagi	7.1	707	45.6
413	MYG003	104	E off Miyagi	7.1	845.4	20.6
414	MYG004	104	E off Miyagi	7.1	1268	46.6
415	MYG006	104	E off Miyagi	7.1	515.7	68.8
416	MYG011	104	E off Miyagi	7.1	1492	19.4
417	MYG012	104	E off Miyagi	7.1	1448	37.3
418	MYG013	104	E off Miyagi	7.1	1049	65.7
419	IWTH02	104	E off Miyagi	7.1	736.5	17.4
420	IWTH04	104	E off Miyagi	7.1	594.8	22.8
421	IWTH05	104	E off Miyagi	7.1	926.8	29.1
422	IWTH21	104	E off Miyagi	7.1	477.2	17.6
423	IWTH23	104	E off Miyagi	7.1	541.9	11.1
424	IWTH26	104	E off Miyagi	7.1	545.1	40.7
425	IWTH27	104	E off Miyagi	7.1	898.4	24.1
426	MYGH03	104	E off Miyagi	7.1	699.7	14.9
427	MYGH04	104	E off Miyagi	7.1	684	20
428	MYGH10	104	E off Miyagi	7.1	768.2	29.3
429	FKS012	105	Fukushima Hamadori	6.7	561.2	55.8
430	FKS013	105	Fukushima Hamadori	6.7	482.5	52.1
431	FKS016	105	Fukushima Hamadori	6.7	543.5	21.7
432	IBR004	105	Fukushima Hamadori	6.7	521.9	13.2
433	IBR013	105	Fukushima Hamadori	6.7	607.8	25.4
434	FKSH12	105	Fukushima Hamadori	6.7	528.6	30.2
435	FKSH13	105	Fukushima Hamadori	6.7	1306	32.6
436	IBRH13	105	Fukushima Hamadori	6.7	570.9	37.3
437	FKS012	106	Eastern Fukushima	5.9	458.3	65
438	FKSH12	106	Eastern Fukushima	5.9	442.7	23.7
439	IBRH13	107	Northern Ibaraki #2	4.9	683.4	26
440	WKYH01	108	Central Wakayama	5.0	1088	26.2
441	WKYH01	109	Central Wakayama	4.3	617.7	12.9
442	IBR003	110	Northern Ibaraki #3	5.1	625.2	10.4
443	IBRH13	111	Northern Ibaraki #4	4.0	540.8	14
444	IBRH14	112	Northern Ibaraki #5	5.0	550.6	8.41
445	IBRH13	113	Northern Ibaraki #6	5.2	722.5	22.2

14 Figures

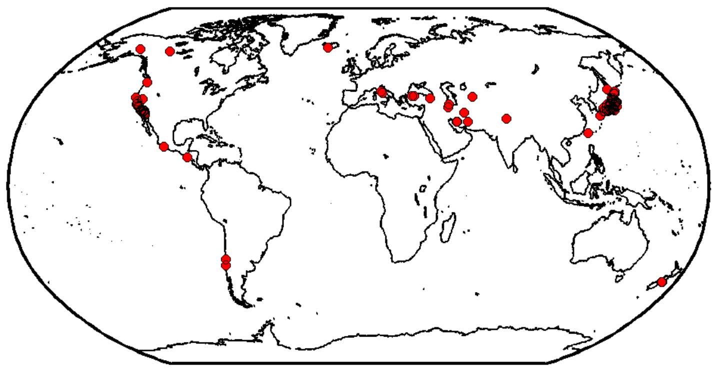

Figure 1: Worldwide locations of earthquakes in the 2013 compilation of exceptional ground motions.

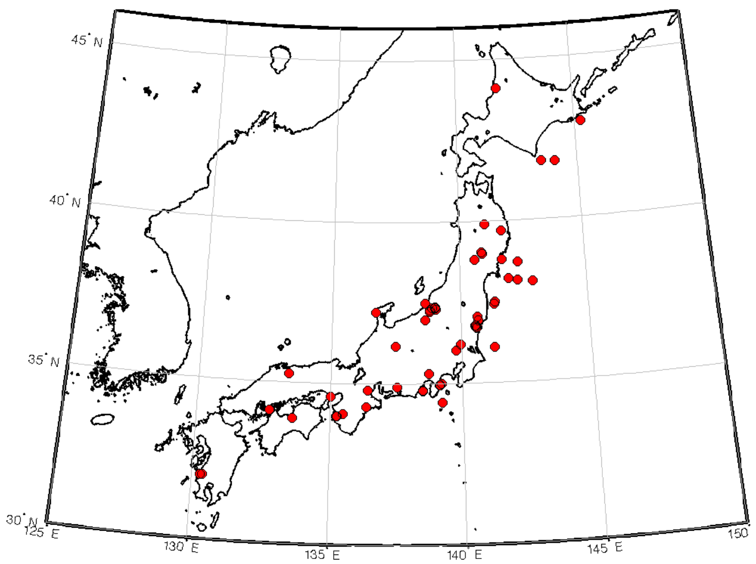

Figure 2: Japanese locations of earthquakes in the 2013 compilation of exceptional ground motions.

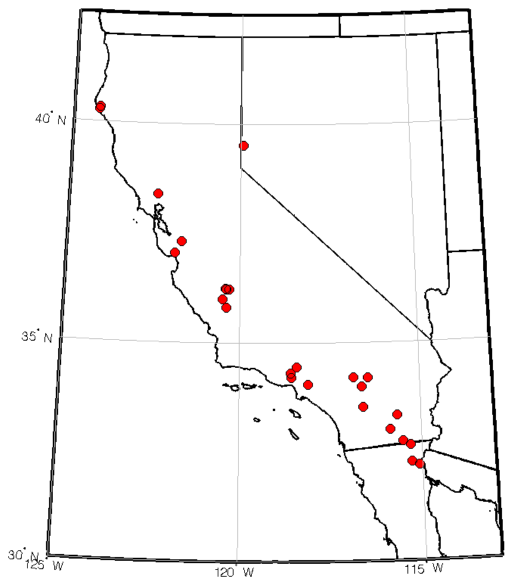

Figure 3: California and Nevada locations of earthquakes in the 2013 compilation of exceptional ground motions.

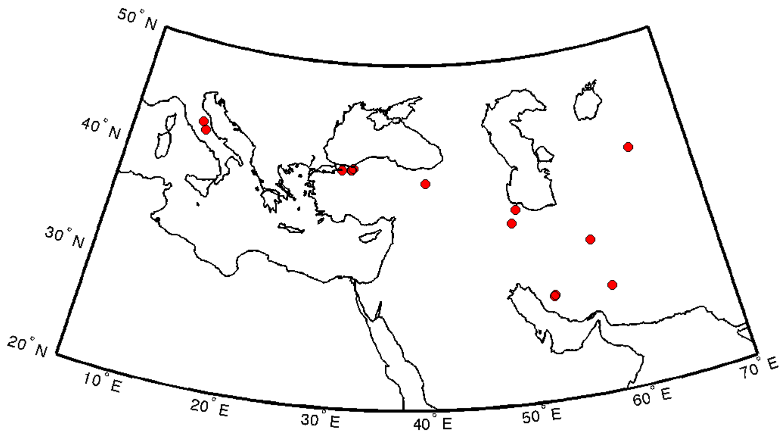

Figure 4: Middle-Eastern and Southern European locations of earthquakes in the 2013 compilation of exceptional ground motions.

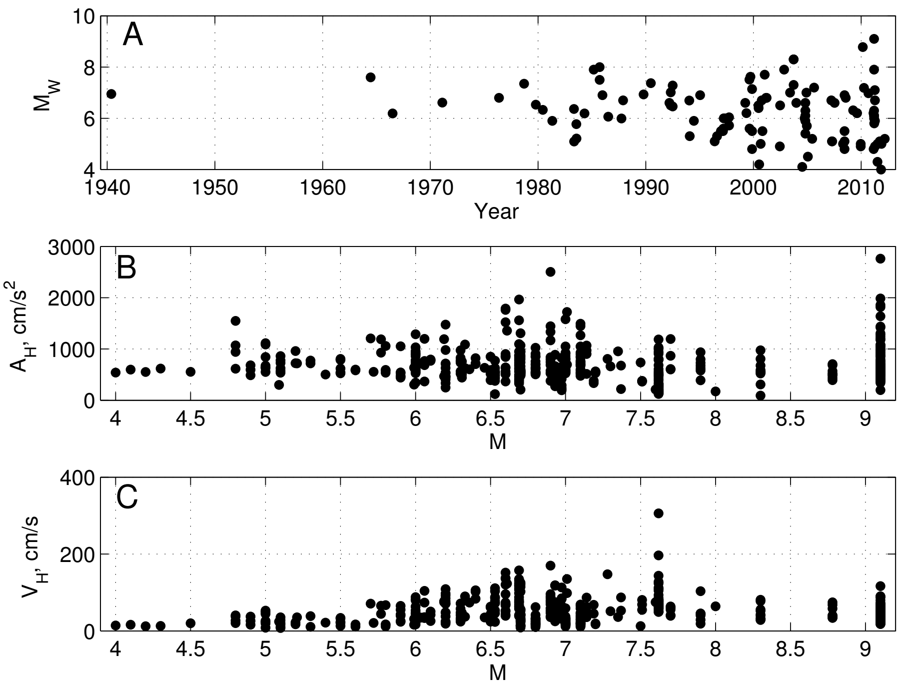

Figure 5: Compilation displayed by (A) magnitude and year, (B) A_H, the maximum horizontal vector acceleration, and magnitude, and (C) A_V, the maximum horizontal vector velocity, and magnitude.

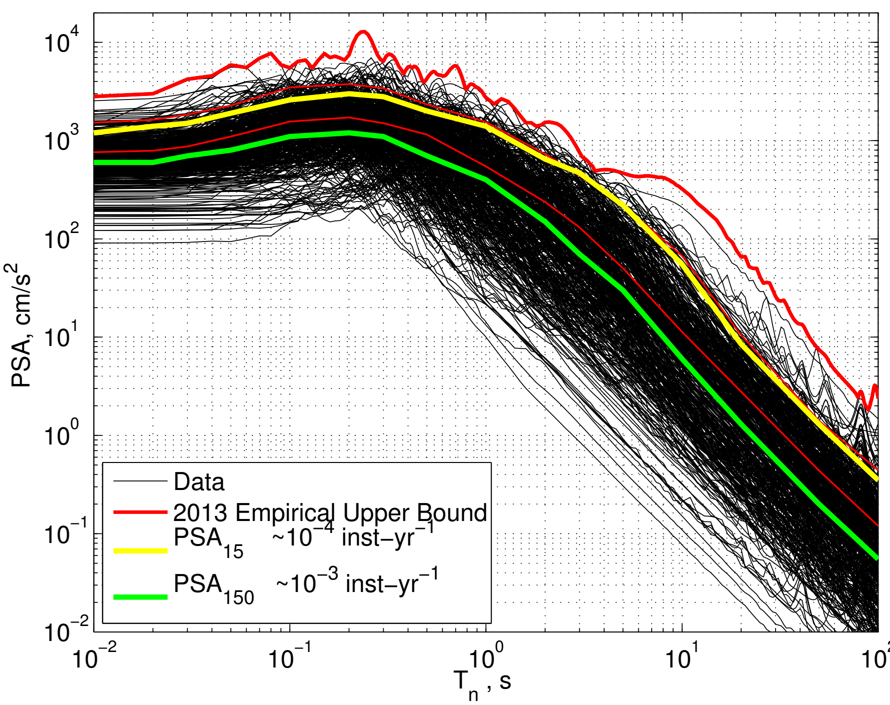

Figure 6: Pseudo-acceleration response (5% damping) of all seismograms in the 2013 compilation. Black lines show PSA_H of each seismogram, calculated at 280 periods between 0.01 s and 100 s. Long period spectra may be underestimated due to high-pass filter applied to accelerograms. Heavy red line shows the current empirical upper bound for the compilation. This line is superimposed on, and hides, the largest spectra. Across the different periods, 18 different accelerograms contribute to this empirical upper bound. The PSA_{15} and PSA_{150} lines are drawn to rounded values that approximate the ranks of 15^{th} and 150^{th} largest response spectra in Anderson (2010). The suggested equivalence of these levels to $10^{-4}/(inst-yr)$ and $10^{-3}/(inst-yr)$ respectively is based on the estimate by Anderson (2010) that the 2010 compilation represented about 150,000 instrument-years. The thin red lines above these show the level of rank 15 and 150 spectra in the 2013 compilation.

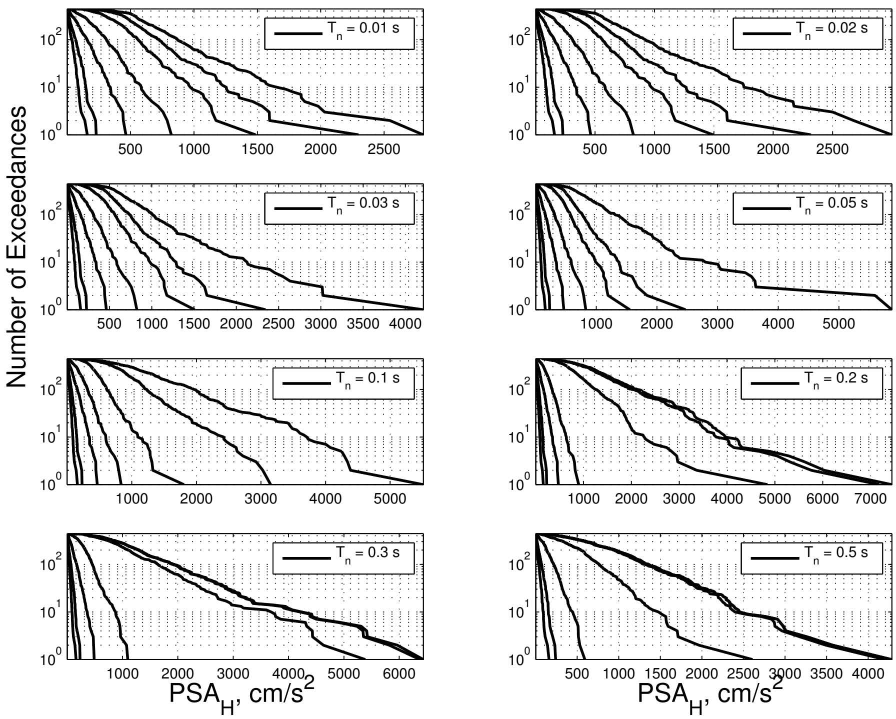

Figure 7: PSA_H (5% damping) distribution at eight short periods. The the ordinate is the number of times that PSA_H is equalled or exceeded in the 2013 compilation. The seven lines show the distributions for seven low-pass filters applied to the seismograms. The filter corner frequencies are, in order of increasing frequency which correspond to lines on this graph from left to right, 0.333 Hz, 0.5 Hz, 1.0 Hz, 2.0 Hz, 5.0 Hz, 10.0 Hz, and unfiltered.

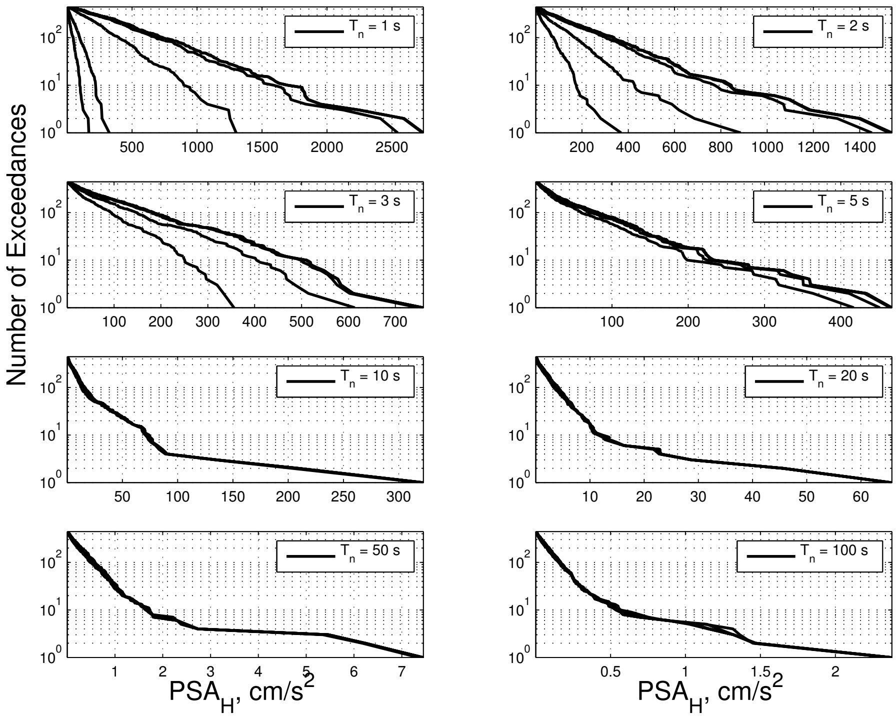

Figure 8: PSA_H (5% damping) distribution equivalent to the distributions in Figure 7, except at eight long periods. The convergence of the lines as the oscillator period increases is the consequence of asymptotic properties of PSA at long periods to values proportional to peak displacement of the seismogram.

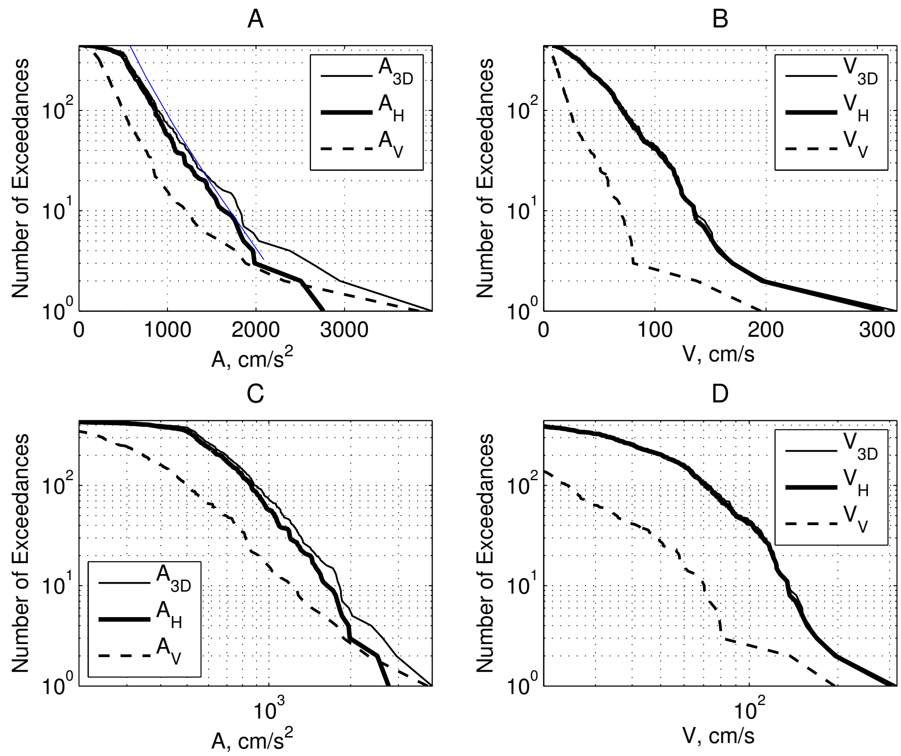

Figure 9: A and V distributions each plotted two ways, to test alternative asymptotic models. The abscissa is the amplitude of A or V, and the ordinate is the number of times that amplitude is equalled or exceeded in the 2013 compilation. For peak velocity, the peak of the 3-dimensional vector is only rarely visibly greater than the horizontal vector. Frames A and B show the distributions on semi-log axes. Frames C and D use logarithmic axes. The extra blue line in Frame A is proportional to the exceedance rate of peak horizontal acceleration from the 2008 National Seismic Hazard of the United States (Petersen et al., 2008) for a location in San Bernardino $(34.11^o N, 117.29^o W)$, as discussed in the text.

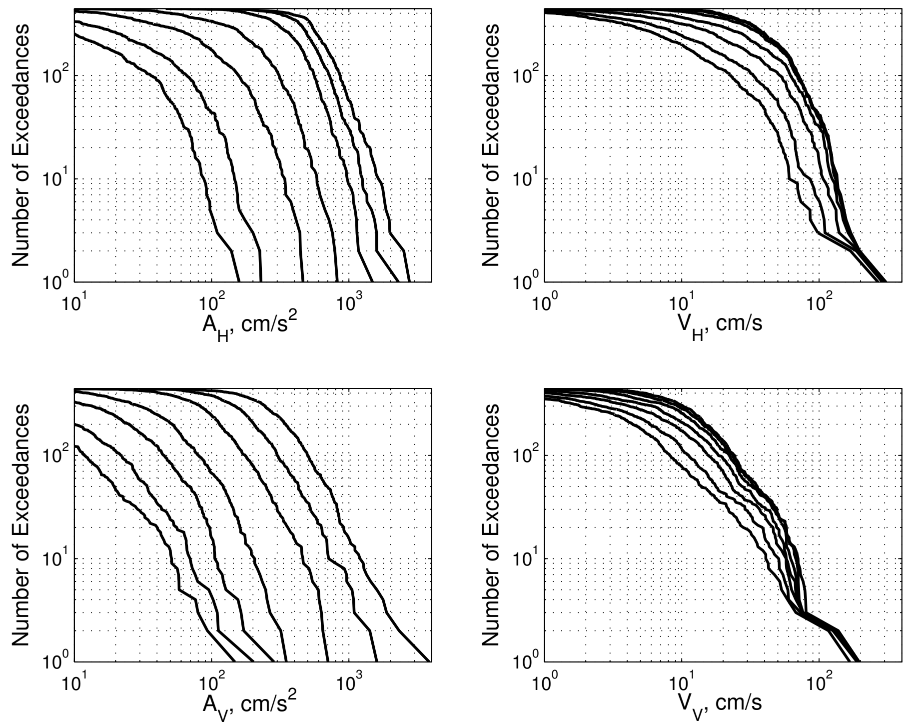

Figure 10: Effect of low-pass filtering on the distribution of horizontal and vertical values of peak acceleration and peak velocity in the 2013 compilation. Filters are the same as those used in Figure 7 and 8.

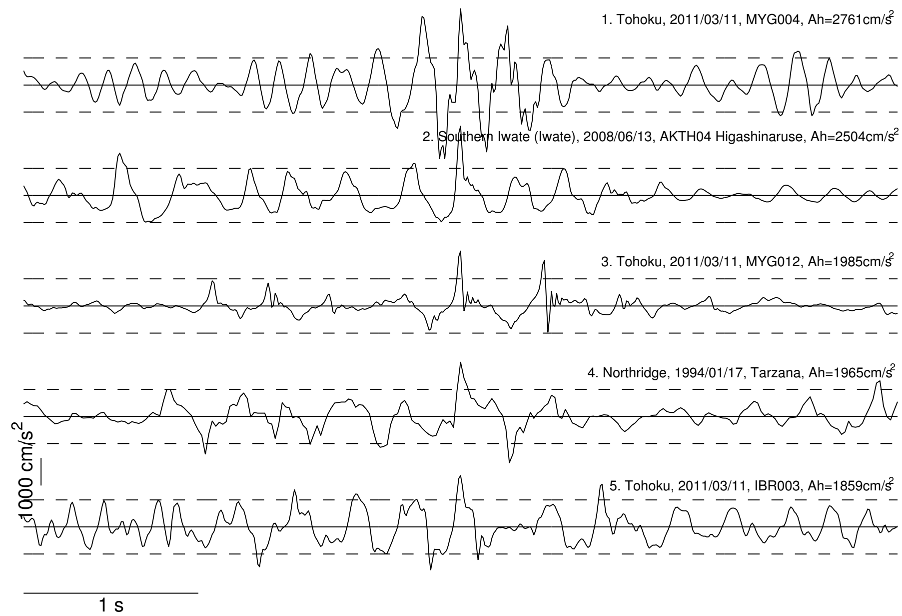

Figure 11: The five largest horizontal accelerations in the 2013 compilation. The annotation above each trace gives the earthquake name and date, the station name, and the orientation. All records are rotated so that this trace has the larged horizontal vector. Dashed lines show accelerations of $\pm g$.

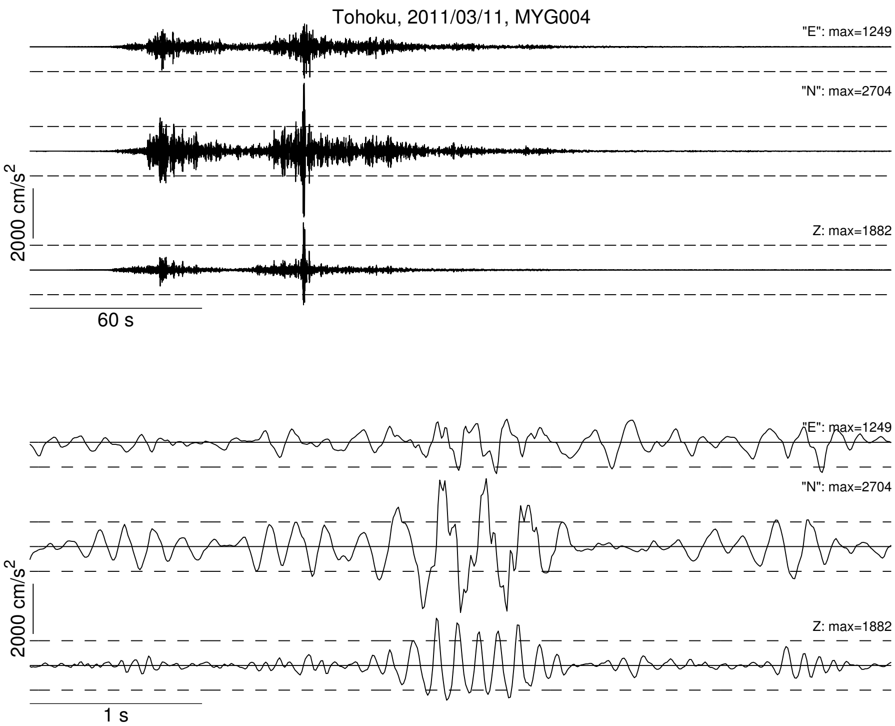

Figure 12: Accelerogram recorded at station MYG004 in the 2011 Tohoku earthquake (M_w9.1). Top: entire accelerogram. Bottom: Segment of 5 second duration centered on time of peak acceleration.

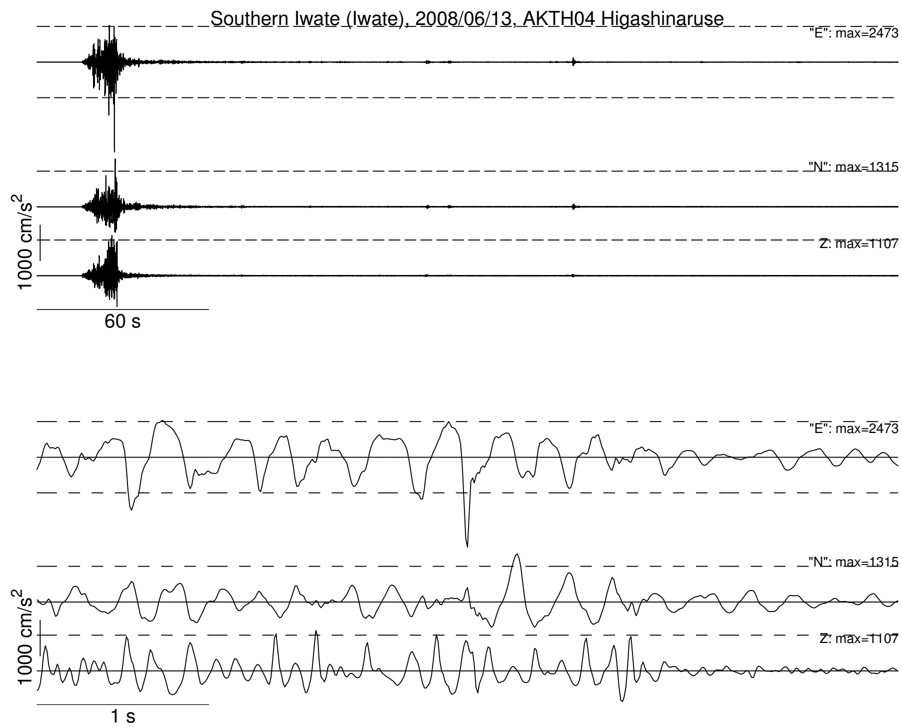

Figure 13: Accelerogram recorded at station AKTH04 in the 2008 Southern Iwate earthquake of June 13 (M_w6.9). Top: entire accelerogram. Bottom: Segment of 5 second duration centered on time of peak acceleration.

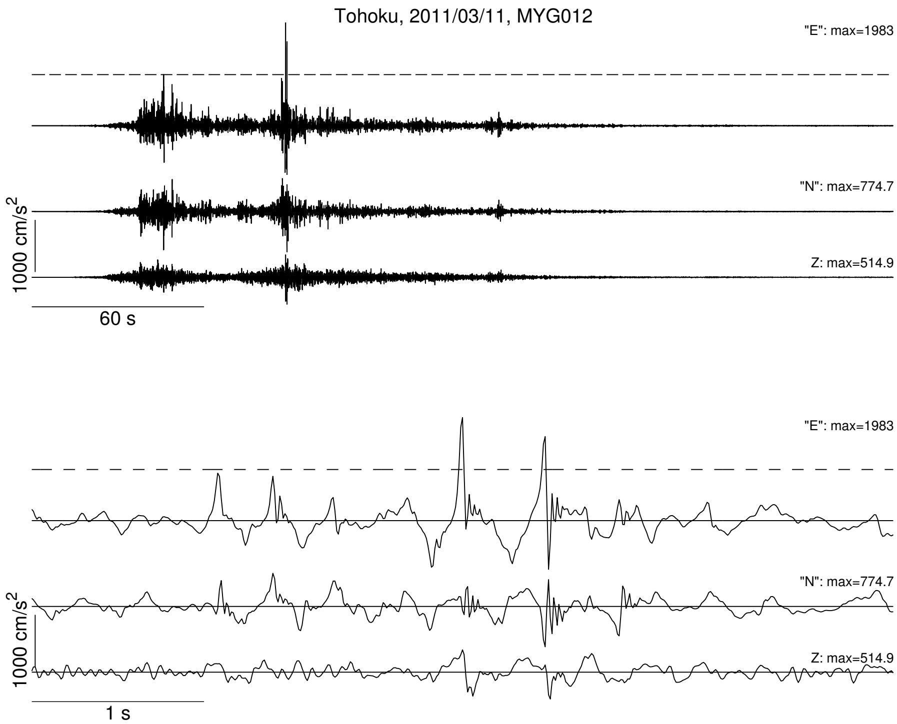

Figure 14: Accelerogram recorded at station MYG012 in the 2011 Tohoku earthquake of March 11 ($M_w 9.1$).

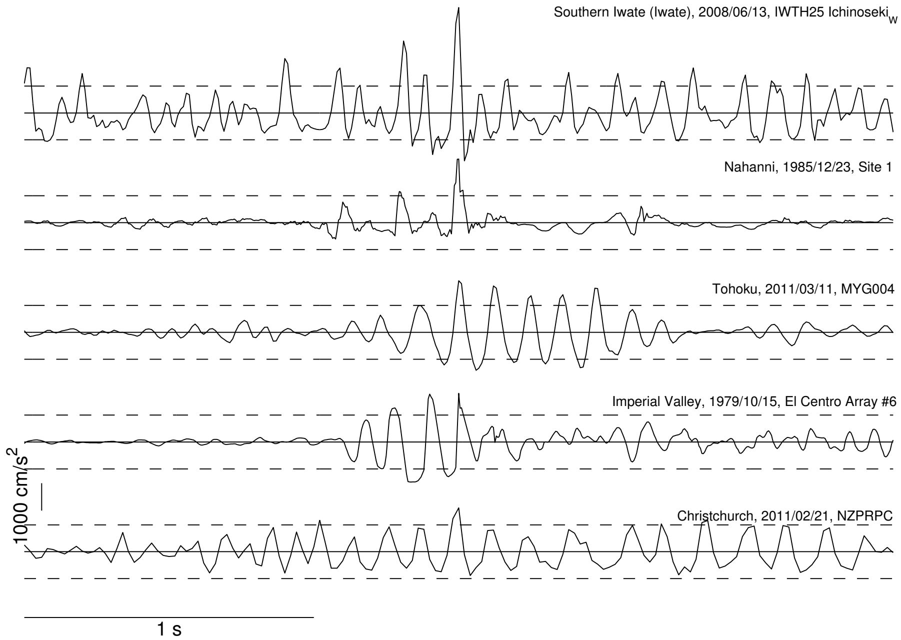

Figure 15: The five largest vertical accelerations in the 2013 compilation. The annotation above each trace gives the earthquake name and date, the station name, and the orientation. Dashed lines show accelerations of $\pm g$.

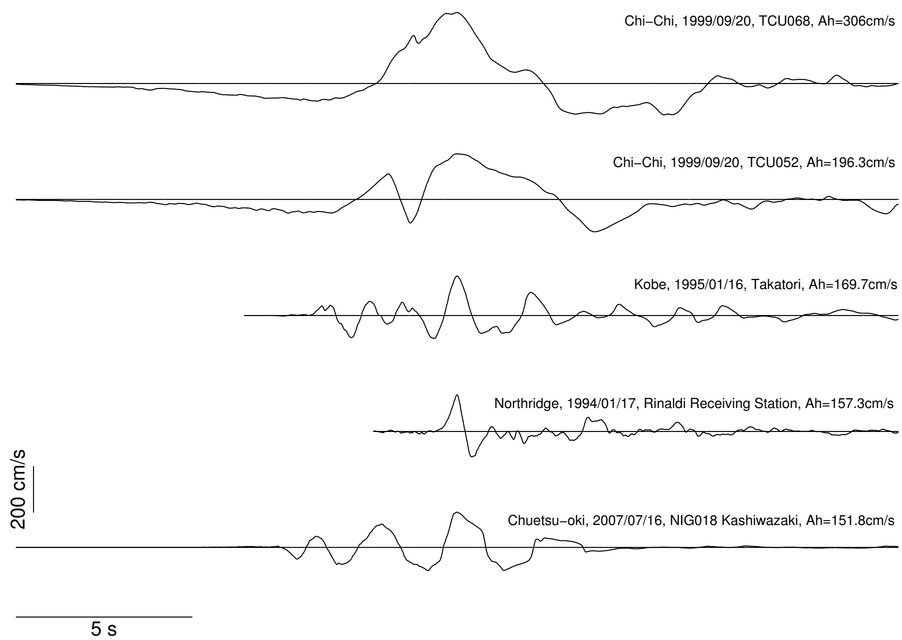

Figure 16: The five largest horizontal velocities in the 2013 compilation. The annotation above each trace gives the earthquake name and date, the station name, and the orientation. Dashed lines show accelerations of ±100 cm/s.

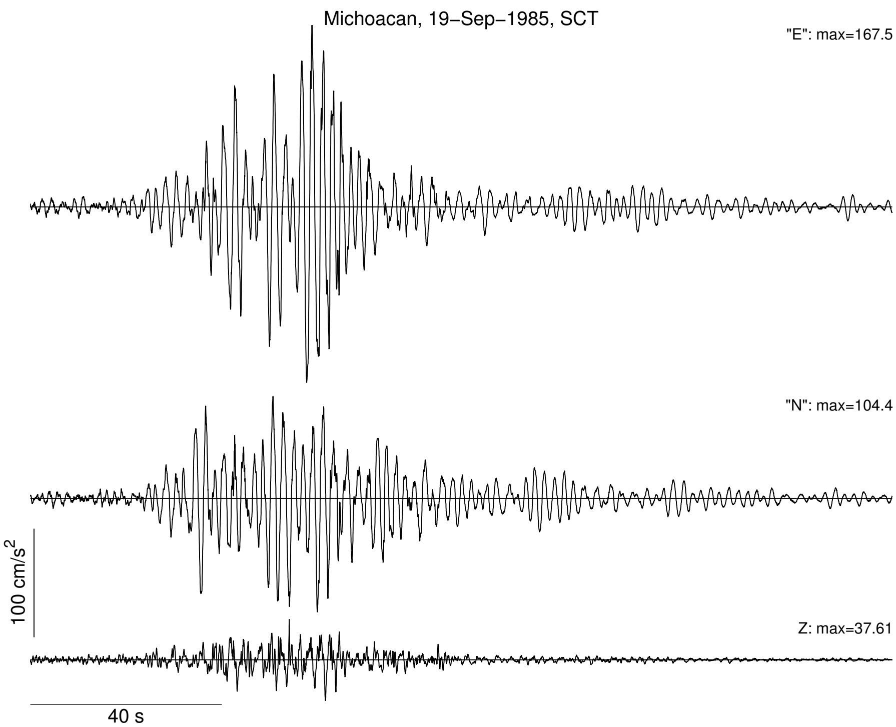

Figure 17: Strong motion recrods from station SCT, recorded in the Sept. 19, 1985 Mexico earthquake (M_w 8.0)

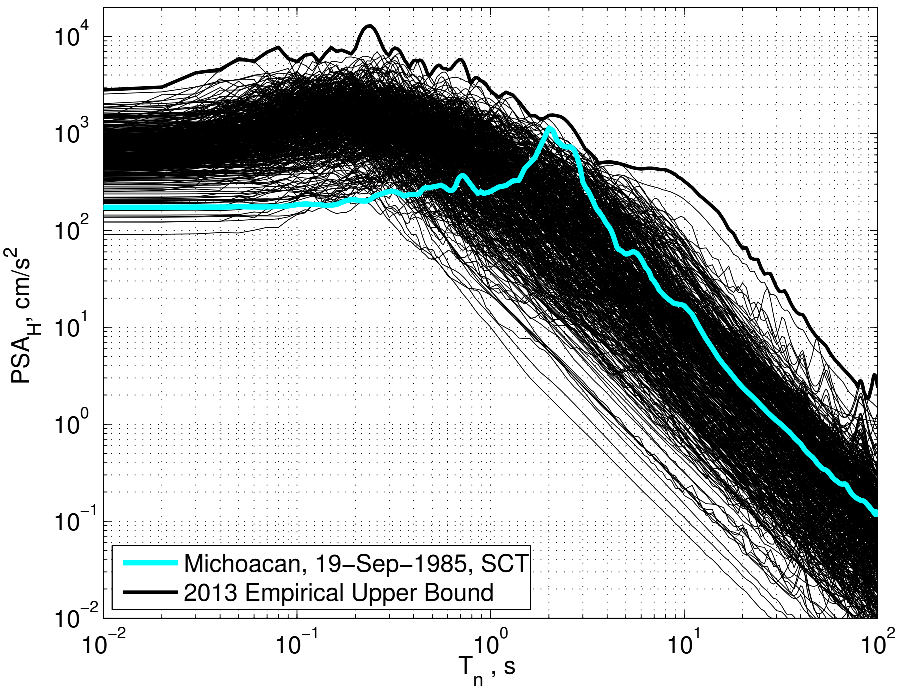

Figure 18: SCT response spectrum, compared with the 2013 compilation of exceptional records.

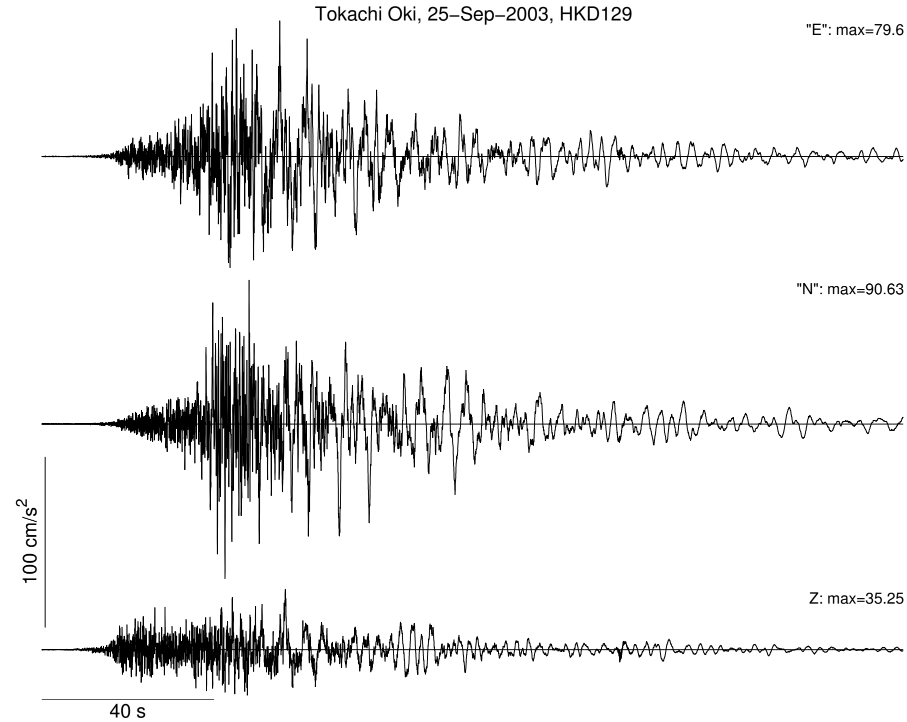

Figure 19: Seismograms from HKD129 in the 2003 Tokachi-Oki Earthquake.

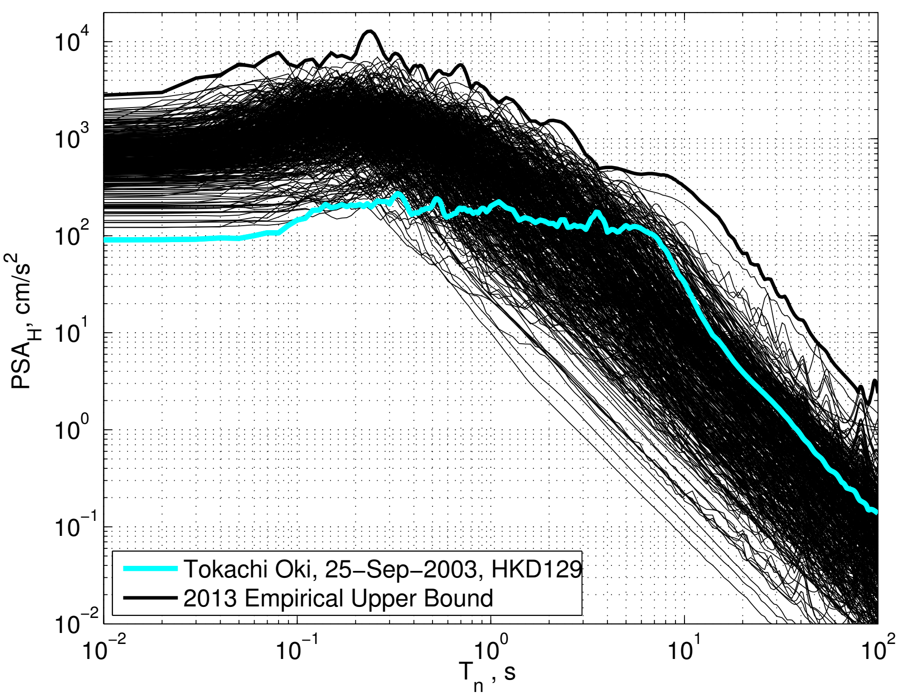

Figure 20: Response spectrum of HKD129 in 2003 Tokachi-Oki earthquake.

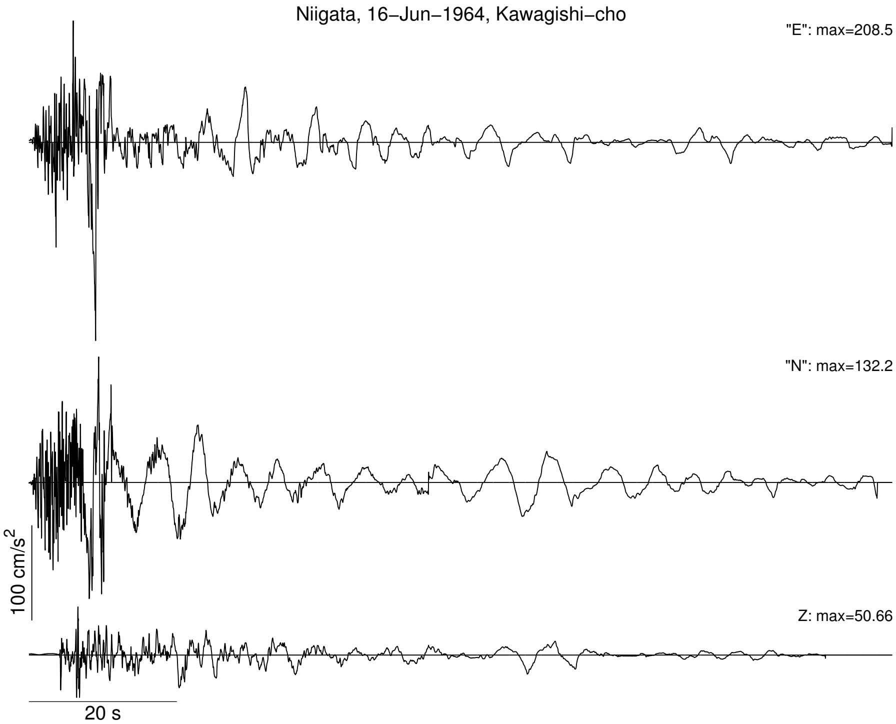

Figure 21: Seismograms of Niigata earthquake, 1964

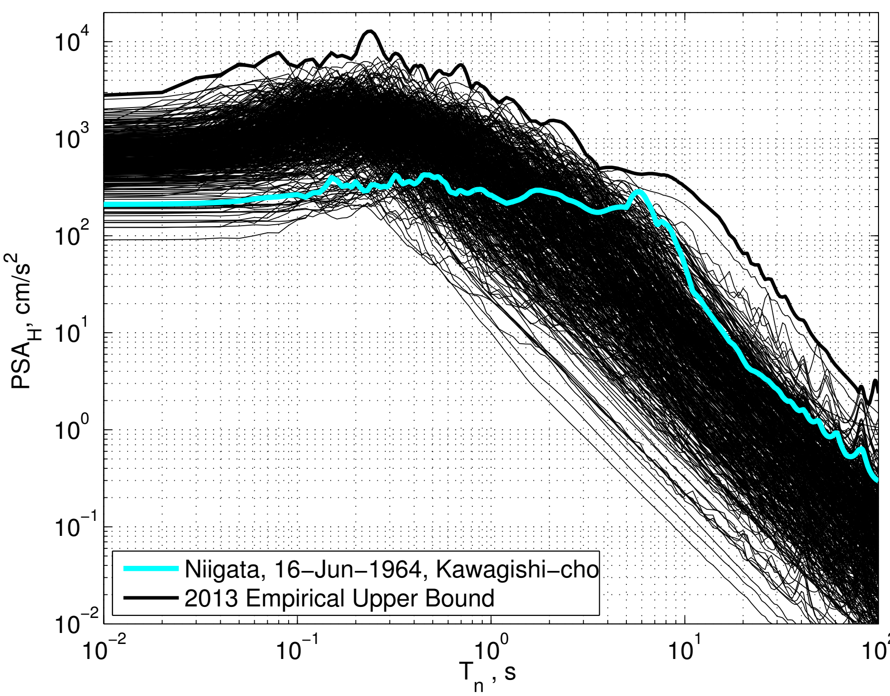

Figure 22: Niigata response spectrum